Combined Experimental and Statistical Model to Understand the Role of Anatomical and Implant Alignment Variables in Guiding Knee Joint Motion

By

Amitkumar Mane

Submitted to the graduate degree program in the Department of Mechanical Engineering and the Graduate Faculty of the University of Kansas in partial fulfillment of the requirements for the Doctoral Degree

Chairperson Dr. Lorin Maletsky

Dr. Ken Fischer

Dr. Carl Luchies

Dr. James Stiles

Dr. Sara Wilson

Date Defended: November 8th, 2011

The Dissertation Committee for Amitkumar Mane

certifies that this is the approved version the following dissertation

Combined Experimental and Statistical Model to Understand the Role of Anatomical and Implant Alignment Variables in Guiding Knee Joint Motion

_____

Chairperson Dr. Lorin Maletsky

Date approved: January 24th, 2012

Acknowledgements

A journey is easier when one travels together. This Dissertation work is the result of six years of hard work of several peoples. It is a pleasant opportunity to thank several peoples who have been helping me in my long journey…..

- Foremost, I would like to express my sincere gratitude to my advisor Dr. Lorin Maletsky. During these years I have known you as a sympathetic and kind person. You always tried to bring the best researcher out of me. You cannot even realize that as a researcher and a person how much I have learned from you.

- Dr. Fischer, Dr. Luchies, Dr. Stiles and Dr. Wilson who always showed enthusiasm in my project updates and were available when I needed their advice.

- DePuy Orthopaedics, a Johnson and Johnson Company, for funding this project.

- My fellow researchers: Chadd Clary, Amber Reeve, Kevin Dodd, Adam Cyr, Mark Komosa, Kaity Fuchinaro and Linda Denny for your late night testing help.

- Most importantly, I would like to thank my girlfriend Jessica for keeping me on track, while working full-time at Zimmer Inc. Thanks for your love along with the encouragement and support when it was most required.

- Last but not the least, my Mom, Dad, brother: Amol and sister-in-law: Swati, who always provided me emotional and mental support. Thanks for providing me the spiritual foundation; without your mental presence in my heart I couldn't have done anything.

Abstract

Kinematics variation is the inheritant part of the joint mechanics; factors such as patient anatomy, joint loading and implant alignments are all variable in nature. The motion patterns of the native human knee joint depend on a combination of its passive motion and the external loads. The former are described by the bony and the ligamentous constraints and the latter depends on muscle activity and external forces to the knee. In order to improve post-surgery knee kinematics, during total knee arthroplasty, the surgeon follows several implant alignment and ligament balancing philosophies. Improvement in the design of orthopedic implants requires a good understanding of the roles that anatomy and implant alignment plays in guiding joint motion. The proposed research focuses on describing the relationship of various anatomical and implants alignment factors with the tibiofemoral kinematics during passive envelope and walk.

An experimental method to manually assess passive knee envelope was described. Principal component (PC) model was developed for the varus-valgus (V-V), internal-external (I-E) and anterior-posterior (A-P) envelope using twenty-one native cadaveric knees and the mode of envelope variations were identified. The Four principal components described about 90% variation in the envelope dataset. First PC summarized about 70% of the variation and was due to the relative position of the envelope, whereas second PC captured about 10% variation describing variation in envelope sizes.

Subsequently, gait simulation was run on seventeen knees using the Kansas Knee Simulator. Effects of variation in V-V and I-E envelope and anatomy on the envelope along with the gait kinematics were assessed using another PC model. Three PCs summarized about 90% variation in anatomy, envelope, and gait kinematics. First PC,

describing 50% variation, captured the envelope and gait kinematics shift combined with the orientation of the epicondylar axis and the origin location of the lateral collateral ligament. Second PC described about 30% variation and was due to the envelope size and the gait range of motion, combined with the epicondylar width and the mediolateral location of collateral origins. Also described was a PC model to predict entire envelope and gait using anatomy and a few envelope measures. Leave-one-out analysis was used and kinematics was predicted with the average RMS error of 2.5º.

Same PC model was used to understand the effect of anatomy and the implant alignment features on the post-TKA envelope and gait kinematics along with the ability to predict the post-TKA kinematics. Four PCs described about 95% variation in the data. Half of the variation was due to the shift in envelope and gait kinematics, combined with the orientation of epicondylar axis and the I-E alignment of the femoral and tibial implant. The second PC described about 25% of the variation and was tied with the size of the envelope, gait and epicondylar width. Tibial V-V alignment affected size of V-V envelope, whereas, femoral I-E alignment was tied with the I-E envelope. Furthermore, PC model was used to predict the envelope and gait kinematics using anatomy and the implant alignment features. Leave-one-out analysis was performed for all predictions and envelope and gait kinematics was predicted and average RMS error was reported.

Table of Contents

List of Abbreviations

aACL	Anterior-medial ACL
ACL	Anterior Cruciate Ligament
A-P	Anterior-Posterior
aPCL	Anterior PCL
CAS	Computer Assisted Surgery
dMCL	Deep MCL
EpA	Epicondylar Axis
EpW	Epicondylar Width
EvM	Envelope of Motion
F-E	Flexion Extension
FPA	Frontal Plane Angle
I-E	Internal-External
LCL	Lateral Collateral Ligament
MCL	Medial Collateral Ligament
ML	Medial-Lateral
MRI	Magnetic Resonance Imaging
pACL	Posterior-lateral ACL
PC	Principal Component
PCA	Principal Component Analysis
PCL	Posterior Cruciate Ligament
PDM	Point Distribution Model
PMC	Posterior Medial Capsule
pPCL	Posterior PCL
ROM	Range of Motion
sMCL	Superior MCL
TKA	Total Knee Arthoplasty
TPA	Transverse Plane Angle
V-V	Varus Valgus

List of Figures

List of Tables

Chapter 1: Introduction

Knowledge of knee joint functional anatomy and the roles that each individual part of structure has in guiding the joint motion is beneficial in designing implants. Numerous studied have been performed to understand the role of soft tissue structure in knee kinematics; however, which part of anatomical structures and how their geometrical arrangements drives knee motion can be further studied. To design and assess surgical procedures for treating knee injuries and diseases, the role of functional anatomy of the joint structures in the kinematics must be understood. During total knee arthroplasty (TKA), geometry of the joint structures and their mechanical properties are often changed. These geometrical parameters include the shape and the size of the articular surfaces and their locations relative to the ligaments and muscle tendon insertions. Similarly, several surgical factors, like, flexion gap, tibial posterior and varus-valgus slope, implant transverse and coronal plane alignment etc, have been identified and thought to affect the post-TKA knee stability and kinematics; however, their interaction with each other and its combine effect on knee kinematics needs to be studied in detail.

The passive motion characteristics of the human knee-joint depend on the mechanical and structural interaction between the articular surfaces, the ligaments and other soft tissue structures. Because of its importance, the passive knee envelope is almost universally used as an intra and post-surgery stability assessment tool; however, the intra-surgery knee assessment could also be influenced by the implant orientation. During dynamic activities like walk and squat, a critical interaction occurs between multiple muscle forces crossing the knee, compressive force at the joint and forces in the passive soft tissue. The relationship between the passive knee envelope and the kinematics during

various functional activities has not been studied thoroughly. It is unclear how the articular geometry and muscle activations of the knee influence the contribution of ligament constraints during dynamic activities. Over last few years, researchers have focused on investigating the importance of a few anatomical factors of the natural and post-surgery knee on a joint motion and stability. These factors include the shape of articular surfaces in natural knees and cruciate and collateral ligaments insertion-origin points in post-surgery knees. Although the information has highlighted the functional implication of these factors on the joint motion and stability, identification and effects of variation of these factors on the joint performance has not been studied thoroughly.

The purpose of the current research was to establish a methodology to understand and characterize the effects of variation in anatomy and implant orientation on passive knee envelope and functional kinematics. Previous efforts have been concentrated to understand the effects of anatomy on kinematics; however these studies lacked the linking of anatomy with envelope and functional kinematics together; the factors which could shed light on several important aspects of knee kinematics. The current research is unique in that from the literature, providing a way to establish a link explaining the effects of variation in anatomical and passive knee envelope factors on kinematics.

In response to these observations, the objectives of the proposed research are to,

1. Correlate natural knee anatomy with observed tibiofemoral kinematics during a passive knee envelope and simulated dynamic activities.
2. Additionally, identify the anatomical and envelope factors that explain the maximum variation in the tibiofemoral kinematics during gait and use them to predict knee kinematics

3. Given a priori anatomical information about the natural knee, estimate the effects of variability in surgical factors, especially implant alignment, on the post-surgery knee kinematics. In addition, identify the surgical factors that explain the maximum variation in the post-TKA kinematics and use them to predict the knee kinematics

In order to accomplish these objectives, following steps were taken. Chapter Two summarizes the literature review of knee anatomy and variation associated with it. Experimental technique to obtain knee passive envelope and the subsequent development of principal component (PC) model to interpret variation in the tibiofemoral envelope is explained in Chapter Three. Obtained results helped characterize the Varus-Valgus (V-V) and Internal-External (I-E) passive envelopes while explaining 90% of the variation.

Chapter Four describes the PC methodology to understand the effect of variation in knee anatomical factors and passive envelope on a functional activity such as gait. Envelope and anatomical factors associated with the variation in the complete envelope and gait kinematics were identified. Furthermore, principal component analysis (PCA) based morphing scheme was developed and the entire envelope and gait kinematics was predicted using anatomical and a few envelope factors. Chapter Five summarized post-TKA envelope and kinematics. After collecting post-TKA passive envelope and gait kinematics, femoral and tibial implant alignments relative to the bone anatomical coordinate frames were calculated. Using PCA, effects of variation in the implant alignment factors, anatomy and envelope factors on the entire envelope and gait kinematics was estimated. A morphing scheme was later used to predict the envelope and gait kinematics.

The final chapter contains concluding remarks about the use of PCA to understand the multivariate knee kinematics. Later part of the chapter discusses overall assessment of the PCA method used in the current study and subsequent suggestions for improving future research.

Chapter 2: Literature Review

The literature review is primarily focused on functional knee anatomy which is thought to influence both passive and active knee laxities and how it changes post-surgery. The additional review provides an introduction to PCA including previously used PC models to interpret a multivariate knee kinematics dataset. The last section of the literature review focuses on the use of PC modeling to perform predictions of bone shapes and its mineral properties using a few principal components.

2.1 Natural Knee Anatomy

A critical interaction between dynamic knee stabilizers, such as muscles, and passive knee stabilizers, such as soft tissue, occurs in stabilizing the knee joint during walking. Further understanding of relationship between the knee passive envelope and the kinematics during various dynamic activities can shed light on the role passive structures play in stabilizing knee joint [1-4]. Despite this information, the anatomical structures that guide the knee motion are not well defined. In order to rank the role of anatomical structures based on their contribution to certain knee motions, the functional anatomy of the knee must be understood. A good understanding of the roles that each individual part of the structure has in guiding the joint motion would help identify the important kinematic-driving factors. The primary constraints to the passive knee envelope are the geometries of the tibiofemoral articular surfaces and the soft tissue structures around the knee joint.

2.1.1 Tibiofemoral Bone Morphology

Since the inception of knee arthroplasty, knee implant systems have undergone significant evolution. Numerous studies on distal femoral and proximal tibial geometry

have improved implant sizing, reducing post-operative problems and extending implant survival rate. These studies have obtained measurement data using a variety of measurement methods, ranging from using vernier callipers to high resolution biplane fluoroscopy. Early studies in the 1970s by Seedhom *et al*. [5], Erkman and Walker [6] and Mensch and Amstutz [7] established the size of many key linear-dimensional variables of the knee, and investigated their relationship, forming the basis of implant geometry. Key femoral anatomical locations are illustrated in Figure 2.1 and related measured values between some of these points listed in Table 2.1. Complementary studies, the findings of which are also shown in Table 2.1, have reported on asymmetry of the distal femur and proximal tibia. In a recent *in vivo* study of two-hundred diverse patients, Rooney and FitzPatrick estimated the correlation of various femoral shape and size variables with ethnicity, gender, and disease state and stage [8]. The group concluded that femoral shape and size variation are strongly correlated to both ethnicity and gender. However, in all groups, epicondylar and trochlear widths of the femur were strongly correlated to the rest of the femoral shape and size variables (Table 2.2). Iwaki *et al.* imaged six cadavers to better understand the shape of articular surfaces and its relevant movement [9]. The group reported that medially, in the sagittal plane the femoral condyle is comprised of the arcs of two circles and that for the tibia it is roughly two angled planes. Laterally, the femoral condyle is composed almost entirely of a single circular facet similar in radius; whereas, the tibia is generally flat allowing anterioroposterior translation of the lateral femoral facet. Similar findings were reported by the Martelli *et al.* [10]; however, unlike Fitzpatrick *et al.* [8], both these groups failed to report the variability within the subjects and the relationship between the tibiofemoral shape

variables with its size. Despite the plethora of knowledge about the tibiofemoral bone morphology, the relationship between knee size and shape variables with knee kinematics has not been reported in literature.

Recent morphological studies have concentrated on identifying one or two 1-D femoral dimensions to represent the size of an entire knee. While studying the resection surface geometry of a knee, Fitzpatrick *et al*. found a positive correlation between femoral epicondylar width and tibial and patellar size variables [11]. Similar results were found by Mahfouz *et al.* [12] and Lavellee *et al.* [13] in their *in vivo* studies. This finding was important and has been used in an automated navigation system like computer assisted surgery (CAS). Lavellee *et al.* developed a statistical model to address the problem of extrapolating very few range data to obtain a complete surface representation of a knee [13]. The group used epicondylar width and interconlylar width points along with a few other random points to represent the femoral size and shape in a CAS system successfully. Although these studies provided revolutionary opportunities to improve knee implant designs, literature doesn't shed light on the effects of variability in tibiofemoral bone morphology on the knee kinematics.

2.1.2 Articular Surfaces

The primary articulation of the knee occurs between the femur and tibia, as the femur rolls across the superior surface of the tibia, so that the contact points are continuously changing. The articulating surfaces of both the femur and tibia are covered with hyaline cartilage, which is composed of a matrix of closely packed collagen fibers. The tibia and femur are separated by the medial and lateral menisci, which are pads of fibrocartilage. They serve as shock absorbers and conform to the shape of the articulating surfaces as the

femur changes position. They also provide lateral stability to the joint and act as a secondary stabilizer to the cruciate ligaments. Both these structures interact to provide joint stability in the knee.

Many studies have been conducted to investigate the topology of the articular surfaces of the femur and the tibia [9, 14-16]. In an *in vivo* MRI study of the twenty adult Caucasian subjects Aoife and FitzPatrick found the thickness distribution of the femoral and tibial articular cartilage [17]. They observed that the femoral cartilage thickness varied along the inner, outer and central lines of both medial and lateral condyles. Whereas, tibial cartilage thickness varied in the mediolateral and anterioroposterior direction of both medial and lateral plateau. But, the study did not exclusively examine the participation of the different parts of the femoral and tibial geometry in guiding the passive motion. Martelli *et al.* studied the shapes of the tibiofemoral articulation and divided it into anterior segments, contacting from 0º-20º of flexion, and posterior segments, contacting from 20º-120º of flexion [10]. The group further investigated the mediolateral and anterioroposterior translation and rotation of the tibiofemoral articular contact point. Researchers have also studied the role of the meniscus in the tibiofemoral articulation [8, 17, 18]. As reported in the literature, the meniscus floats between the tibiofemoral articular cartilages during 30º-120º of flexion range [18]. For the flexion angles less than 30º, the medial condyle of the femur pushes more on the anterior horn of the medial meniscus and experiences anterioroposterior constraint. Whereas, for the flexion angles greater than 120º, the lateral meniscus is trapped between the tibiofemoral articular surfaces producing a considerable resisting force. In the basic and simplified model Amiri *et al.* attempted to understand the role of tibial articular surfaces in guiding

the passive motion [19]. The group subsequently concluded that the medial meniscus promoted the tibial internal rotation and restrained the femoral posterior translation; whereas, the lateral meniscus and the medial aspects of the tibial eminence was found as the elements that confined the tibial internal rotation. In summary, current available literature provide insight about the shape and size variation of the tibiofemoral articular surfaces and role of the meniscus in guiding knee motion; however, this does not explain the effect of intra-subject anatomical variation of articular cartilage on knee kinematics during active or passive motions.

2.1.3 Ligaments

The passive motion characteristics of the human knee joint depend on the structural interaction between the articular surfaces and the ligaments. Because of the relative incongruency of the articular surfaces, the ligaments play an important role in providing the passive stability of the joint. The term 'stability' is widely used in the literature; however, a very few authors have quantified the term. In his review article, Engh defined joint as a stable joint if a knee can open 3mm when V-V moments are applied [20]. Whereas, O'Conner and Goodfellow defined stability as a measure of the degree to which relative movement at the bearing surface is limited or resisted [21]. Although TKA is a well-established procedure that generally results in pain relief and a high level of patient satisfaction, post-TKA instability is one of the most common causes of the TKA failure [15, 22-24]. Several studies reported that the post-TKA instability might be due to the inadequate correction of soft tissue imbalances in both sagittal and coronal planes [22, 23, 25-27]. In the native knee, sagittal plane stability is maintained by the cruciate

ligaments, whereas in both native and post-TKA knees, frontal plane stability is controlled by the collateral ligaments.

2.1.3.1 Cruciate Ligaments

Sagittal plane stability of a knee is achieved by two cruciate ligaments: the anterior cruciate ligament (ACL) and the posterior cruciate ligament (PCL). The ACL is attached to the cavity in front of the spine of the tibia and passes obliquely superior, posterior and laterally, inserting into the inner and posterior part of the lateral femoral condyle. The PCL is attached to the posterior cavity of the tibial spine and passes superior, anterior and medial to the medial condyle of the femur. Both of these ligaments are further subdivided into two bundles. They include the antero-medial (aACL) and postero-lateral bundles (pACL) of the ACL along with the anterior (aPCL) and posterior (pPCL) bundles of the PCL. Several studies have been performed to understand the biomechanical behavior of cruciate ligaments and their role in passive knee motion. In their mathematic model, Butler *et al.* recognized the complex multifiber bundle morphology of both cruciates and have suggested that each bundle has unique biomechanical roles in controlling tibiofemoral kinematics [1, 2, 28]. Another analytical model developed by Yu *et al.* helped divide the flexion range and identify the role of each cruciate during that flexion range [1]. The group found that for passive range of knee motion all of the cruciate ligament bundles were loaded with the joint positioned between 0º-10º of knee flexion. However, passive flexion of the knee from 10º-50º caused the aACL and the pACL, along with the pPCL to slack or unload, indicating minimum contribution of cruciates. After 50º of knee flexion, anterior bundles of both the ACL and PCL became tensed indicating their active recruitment. Similar results were observed by Temelli *et al.*

[29] and Blankevoort *et al.* [2]. While studying the recruitment of a knee ligament, Blankevoort and associates found that both bundles of the ACL and the posterior bundle of the PCL were engaged during tibial internal rotation. Whereas, only the anterior bundle of the PCL was recruited with tibial external rotation at higher flexion angles (>90º). In an *in vivo* study with eight patients, Li *et al.* used dual fluoroscopy to measure free lengths of both cruciates during deep squat [30]. The group reported increases in the lengths of the aPCL and pPCL bundles with flexion from 0º to 120º and decreased beyond 120º of flexion. The femoral attachment of the posterior cruciate ligament twisted externally with increasing flexion and reached a maximum of 86.4º ± 14.7º at 135º of flexion. However, Li *et al*. didn't report the effects of the variation in the ligament origin-insertion sites on the knee stability and kinematics.

2.1.3.2 Collateral Ligaments

Coronal plane stability of a knee is partially maintained by two collateral ligaments: the medial collateral ligament (MCL) and the lateral collateral ligament (LCL).The MCL has multiple origin and insertion sites and spans the medial aspect of the knee. It is divided into three distinct components: the superficial MCL (sMCL), the deep MCL (dMCL) and the postero-medial capsule (PMC). The primary function of the MCL is to resist valgus torques applied to the tibia, although it is a secondary restraint to anterior-posterior force and internal-external torques. Different structures and different bundles of the MCL come into play at different degrees of knee flexion to stabilize the joint. A ligament recruitment study performed by Blankevoort *et al.* observed that the dMCL was recruited over the entire flexion range, whereas the PMC was slack for flexion angles greater than 60º [2]. Of the dMCL, only the posterior portion was loaded between

extension and 20º. In a similar study performed by Ahmed *et al.*, the MCL was found to be a supporting restraint to internal rotation [31]. The group measured tension between the MCL for internal-external rotation and found a gradual increase in MCL tension from external to internal rotation. On the lateral aspect of a knee, the LCL originates from the femur and insert on the fibula. The LCL is a primary restraint to the varus and external tibial rotations. Further extending the study from the MCL, Blankevoort *et al.* observed that the posterior portion of the LCL was not recruited beyond a certain flexion angle, which was variable among the tested joint specimens [2, 3]. However, at full extension and under anterior-posterior loads of ±30N, the LCL was extremely tight indicating constraint to the anterioroposterior motion. In another *in vivo* study of five subjects, Li *et al.* attempted to measure free lengths of collateral ligaments using dual fluoroscopy [32, 33]. They found that the length of the sMCL did not change significantly with flexion, the length of the PMC consistently decreased with flexion and the change in length of the dMCL with flexion was similar to the trend observed for the sMCL. The length of the anterior aspects of LCL increased with flexion and posterior bundle decreased with flexion. The group concluded that the collateral ligaments did not elongate uniformly as the knee was flexed, with different bundles becoming taut and slack.

Several mathematical and computational models have shown that both cruciate and collateral origin and insertion points have a prominent effect on the kinetic and kinematics model output quantities, while stiffness and initial strain condition of the ligament bundles had less of an effect on the model outputs [2, 10, 22, 29]. Temelli *et al.* observed that the output of his mathematical knee model was sensitive to the small variation in the insertion-origin location of ACL, sPCL, dPCL, MCL and LCL [29].

Similar behavior was observed by the Beynnon *et al.* who developed a sagittal plane model of a knee using sensitivity analysis [1]. All these studies raised a concern about the efficacy of computational modeling to the ligament free length and its attachment sites. Therefore, further understanding of the link explaining the variability in ligament origin-insertion locations and its effect on knee kinematics would be useful.

2.2 Total Knee Arthroplasty

Total knee arthroplasty is a procedure to replace the degenerated and osteoarthritis knee articular cartilage by tibial and femoral prostheses. Although successful in pain relief, the procedure does not ensure post-surgery knee stability during various functional activities [34, 35]. Several factors have been identified that affect the post-surgery performance of a joint. Some of these major factors are: surgical management of soft tissues, prosthesis design features and its alignment.

2.2.1 Modifications in Total Knee Arthroplasty

It is well established that the long-term results of TKA are influenced by the immediate postoperative restoration of proper ligamentous stability and implant alignment. Adequately managing or balancing of the soft tissue is a key factor in achieving a successful TKA. Post-operative malalignment or imbalance of the collateral ligaments can lead to a lax joint and result in early loosening and instability, and leaving the knee too tight may cause stiffness and limited motion. Delp *at al.* defined coronal plane stability as 6º of overall varus-valgus range of motion and less than 3º differences in varus or valgus motions from unloaded or 'neutral' alignment [36]. In a retrospective study, Engh *et al.* defined stability as relatively equal tension on the medial and lateral sides of the knee with the mechanical axis passing through the center or slightly lateral to

the center of the knee [20]. These stability criteria are useful while operating on knees with fixed varus-valgus deformities. It is accepted that release of the lateral soft tissue, iliotibial band and LCL, is needed for the correction of a valgus deformity. However, the procedure of the medial release for the correction of a varus deformity remains a matter of discussion.

Ligament balancing also plays an important role while defining tibiofemoral bone resection surfaces and subsequent implant alignment. In a rectangle flexion gap method, a gap between posterior femoral cuts and distal tibial cut at 90º flexion angle is achieved; whereas, at in a rectangle extension gap, a gap between distal femoral cuts and proximal tibial cut at full extension is achieved. Surgeons use various philosophies to obtain these rectangle gaps; by collateral ligament release, re-cutting bone cuts or using thicker tibial inserts. Failure to achieve the rectangular gap at full extension and 90º of flexion leads to limb misalignment and is considered a symptom of varus or valgus knee deformity. To increase the accuracy of flexion-extension gaps, surgeons have used various methods. Kurosaka *et al.* used a navigation system (CAS) to evaluate the flexion-extension gap at various flexion angles instead of only at full extension and 90º of knee flexion [25, 37]. The group reported varying joint gap with flexion angle and recommended necessary changes in either implant design or surgical procedure or both. Matsueda *et al.* reported the gradual effects of resection of various medial and lateral soft structures on flexion gaps at 0º and 90º of knee flexion [26]. Both, the joint gap and the frontal plane alignment, were more sensitive to the medial release sequence than the lateral. Although the information is useful to understand importance of joint gap, both these authors did not report the relationship between tibiofemoral kinematics or tibial frontal plane alignment

and flexion-extension gap. The knowledge of the variability in flexion gap and its subsequent effects on the specific tibiofemoral kinematics will help correlate the surgical variables with post-TKA knee stability and performance.

Several authors have suggested that altering the rotation of the femoral component during TKA may significantly improve both tibial and patellar tracking with minimum complications [24, 38, 39]. Particularly, Rhoads *et al.* [40], Figgie *et al.* [24] and Anouchi *et al.* [39] concluded that a small amount of femoral external rotation improves tibiofemoral kinematics. With neutral alignment defined as equal resection of the posterior femoral condyles, external femoral rotation decreases the dimension of posterior medial condyle and increases the lateral condyle, and would be expected to cause varus positioning of the tibia relative to femur. Moreover, the external femoral alignment decreases the lateral flexion gap without creating an abnormally increased medial flexion gap or abnormal stress in the lateral ligaments. Tibial slope in the frontal plane is also an important factor. In order to maintain a 3º varus slope, perpendicular resection of the proximal tibial surface usually removes more bone from the lateral tibial surface than the medial surface [41, 42]. Rotational position of the femoral component is likely to interact with this slope and affect the flexion-extension gap, which is later corrected by the further ligament balance. These interacting and iterative relationships between ligament balance, bone resection surfaces and implant alignment are thought to affect the knee stability and alignment during both passive and active motions of a knee. Although several surgical factors, like flexion gap, tibial posterior and medial-lateral slope, implant transverse and coronal plane alignment etc., have been identified and

thought to affect the knee stability and kinematics, their interaction and effect on knee kinematics have can be studied further.

2.2.2 Knee Envelope as an Assessment Tool

The motion patterns of the human knee joint can be partially explained by its passive motion characteristics, which are described by the ligaments and the bony constraints. The relationship between the passive knee envelope and the kinematics during various dynamic activities has not been studied thoroughly. It is unclear how the articular geometry and muscle activations of the knee influence the contribution of ligament constraints during dynamic activities. In a native knee, biological arrangement of the soft tissue structures and the articular surfaces drive the passive motion. Knee kinematics collected from the passive envelope assessment could therefore be used to identify the role of various soft tissues in driving motion of a native knee. This information could be crucial to compare post-TKA stability, which is maintained by the ligament balance and the implants' design features.

Because of its importance, the passive knee envelope is almost universally used as an intra- and post-surgery stability assessment tool. Knee stability has important functional implications; thus, understanding how total knee arthroplasty changes the knee stability and how that change is related to surgical technique is an important step towards improving surgical reconstructions. Several authors have attempted to approach knee stability from a knee laxity point of view, which can be evaluated using knee passive envelope of motion [28, 39, 43]. Previous researchers have studied a knee laxity intra-operatively using surgical navigation system like CAS [28, 40], on live patients using manual loading [44] and on cadavers using various loading devices [3, 22, 45]. The

comparison of post-surgery envelope with pre-surgery may highlight the factors responsible for the reduced post-surgery knee stability.

These studies provided meaningful information about knee joint laxity; however, they failed to establish the link between passive knee motion and active kinematics like walk and squat. Therefore, a method of evaluating success of TKA using intra-surgical envelope assessment could be inadequate and could fail to predict functional outcome of a surgery. Keeping this gap in mind, Freeman *et al*. attempted to understand the relationship between passive envelope and load-bearing *in vivo* squat [46]. In seven loaded living knees with the subjects squatting, the relative TF motions were similar to those in the unloaded knee. Also, characteristics motions, tibial internal rotation, posterior femoral translation and femoral facets 'Lift-off', with knee flexion were observed. The group concluded that the similar soft tissues and functional constraints like articular geometry drives both passive motion and weight-bearing squat. Andriacchi *et al*. tested thirty-five subjects to understand the interaction between active and passive knee stabilizers during level walking [47]. The results demonstrated that both muscle forces and soft tissue recruitment played important role in maintaining joint stability during stance phase of a gait. Although the study shaded a light on the relationship between knee constraints during level gait, authors did not talk summarize the trends of passive flexion and its association with gait kinematics. Therefore, understanding link between passive knee motions and functional activities could provide unique piece of information.

2.3 Principal Component Modeling of a Knee

Principal component analysis is a statistical tool that has become quite popular in the analysis of multivariate data. The aim of a PCA is to reduce the dimensionality of a

multivariate data set while retaining as much variation as possible. The original variables are transformed into principal components. The Principal Components (PCs) are linearly independent of one another. The first PC is a linear function of the variables, which has maximum variance. The second PC is a linear function of the variables, orthogonal to the first PC, which has maximum variance. This was described geometrically by Jolliffe in terms of two variables [48]. If there are just two variables they could be plotted on an x-y graph. A linear equation for x could be written in terms of y, and similarly a linear equation for y could be written in terms of x. but these two equations would be different as they are involved in reducing the distance from the points to the line in either the x- or the y-direction but not both, and assume one independent and one dependent variable. The first PC defines a best-fit line to the points, which reduces the perpendicular distance from the points to the line. The second PC is a line orthogonal to the first (Fig. 2.2). If an ellipse was drawn around these points the major and minor axes of the ellipse would be the first and second PCs respectively. The higher the correlation between x and y, the more variation there will be along the direction of the first PC and the less there will be along the direction of the second PC. This theory can be expanded to include multiple variables.

The number of PCs will be equal to the number of variables, but each subsequent PC will be orthogonal to the previous PCs and will be responsible for less variation than the previous PC. If a set of variables have substantial correlations among then, the first few PCs will account for most of the variation in the original variables. For a PCA to give any useful results, this must hold true with a number of PCs that is significantly fewer than the number of original variables explaining most of the variation. Interpretation of PCs is

one of the most important steps in PCA. The sign of a PC coefficient is usually arbitrary, what is important however, is the sign of a PC coefficient relative to the signs of the other coefficients in the PC. If PC coefficients have the same sign, it relates to the variability that the variables have in common. If PC coefficients have different signs it relates to differences in variability. If, for example, a principal component has nearly equal coefficients of the same sign, the PC is a weighted average of all variables. An increase in one variable is matched with an increase in all other variables and similarly a decrease will affect all variables equally. In terms of anatomical or biological measurements, this PC is usually associated with the size of the specimen. In other PCs there are usually two groups one containing the positive coefficients and the other containing the negative coefficients of non-negligible magnitude. An increase in the proportions of the variables of one group is matched by a decrease in the proportions of the variables in the other group. In anatomic terms, PCs with coefficients of the same sign describe size variation in the specimen, as all dimensions are varying in the same direction; PCs with coefficients of different signs describe shape variation in the specimen.

Several authors have demonstrated the usefulness of PCA in knee biomechanics to reduce the dimensionality and explain inter-subject variability of the gait waveform. Deluzio *et al.* first introduced the concept to PC modeling in knee biomechanics by comparing net reaction force and flexion angle of normal and pathological gait patterns [49]. In following studies, the group further developed the model and attempted to understand the frontal plane dynamics and loading response of native and unicompartmental gait cycles [50]. Since then, a number of researchers used PCA to compare several waveforms of normal and pathological patients. Epifanio *et al.*

compared knee flexion-extension angle and moment during sit-to-stand waveforms [51]. Sadeghi *et al.* first developed a simple PC model to study the underlying structure of power developed by flexors/extensors of the hip in able-bodied gait [52]. In a follow-up study the group used PCA to compare the functional roles of hip flexors/extensors between right and left limb [53]. Although these authors used PCA to compare normal and pathological kinetics/kinematics, PC interpretation was not performed in their studies. This PC interpretation with gait kinematics/kinetics was performed by Beynon *et al.*, who addressed the variability in knee flexion-extension, varus-valgus and internal-external rotation angle along with anteroposterior and vertical reaction force at knee during stance phase of a gait [54]. The group further interpreted the first few PCs of each input variables and correlated them with either the reaction force magnitude or the percentage of stance phase.

2.3.1 PC Modeling, a Prediction Tool

In many existing CAS-systems optical localizers are used to acquire scatter point data on patient's bone surface in order to create a patient specific bone model. Several statistical models have been developed to build a complete surface model from sparse data; however, Point distribution model (PDM) proposed by Coots and Taylor is a widely accepted model [55]. The method first uses a training dataset to estimate the mean shape of the surface. Modes of the variations, PCs, are found using PCA on the deviations of the training set from the mean. These modes or PCs are represented by orthogonal eigenvectors. A new shape is generated by adding linear combinations of the most significant variation vectors to the mean shape. In other words, in a PDM algorithm, the sets of points are aligned to minimize the variance in distance between equivalent points

on mean shape model. Since for each PC, the deviation of mean shape within ±3σ of the training shapes can be obtained, PC interpretation becomes relatively easier.

Mahfouz *et al.* used PDM and PCA to estimate the difference between male and female femur shapes [12]. The group also correlated each PC with the femoral surface and demonstrated exactly which portion of the femoral surface is sensitive to the gender differences. FitzPatrick *et al*. used the similar approach to interpret the size and shape of the resection surface geometry of the orsteoarthritic knee [11]. Their model explained the variability of the tibiofemoral bone cuts on fourteen subjects. The variation of mean resection cuts within ±3σ for first two PCs demonstrated that first PC was a resection cut size variable, whereas second PC was associated with the posterior femoral cuts which could lead to overhang or underhang of the femoral implant.

2.3.2 PCA Optimization

Numerous PCA optimization routines have been used successfully to predict outcome from a-priori knowledge. The 'Hand crafted' models, articulated models, active contour model, Fourier series model, statistical shape models are a few of the optimization routines. All these models attempted to obtained complete output parameters using a few input parameters. Statistical models were widely used for constructing a patient specific 3D surface using small subset of digitized points [56]. Several statistical models were developed to predict the bone shape; however, very few of them allowed interaction between spatial, such as bone shape, and non-spatial, such as age, BMI, gender etc.

Styner *et al.* derived a scheme operating directly in the PCA shape space incorporating a large set of possible variations including parameters additionally to spatial information such as patient height, weight and age [39]. The optimization method

was based on the iterative removal of shape information associated with the digitized points. During the optimization, the group calculated the most probable shape subjected to the boundary conditions that are related to the initial digitized landmark. The resulting outline was used for registration and as an initial configuration for computing the most probable shape for the next digitized point. Using shape analysis, the group examined the remaining shape variability after the surface information coded by the digitized points was progressively subtracted. The procedure was repeated until all digitized points were used to obtain the final bone shape. The optimization procedure offered the benefit of including non-spatial information. Therefore, this optimization algorithm can be used to predict a dataset in spatial space, using a few non-spatial parameters.

Despite the wide range of applications of PCA in knee biomechanics, almost no study in the literature addresses the use of PCA to interpret passive or active knee laxity and variation associated with it. The PC modeling provides huge potential to well interpret and understand the knee kinematics. Also, with enough training sets of passive envelopes, the mean size and shape describing entire variation in the motion can be obtained. Several anatomical factors, which are thought to affect the passive envelope of knee, and their variability can be associated with the knee kinematics. The method can be further used to identify factors responsible for specific knee motion and their ranking based on their influence of variability on a knee kinematics.

2.4 Figures

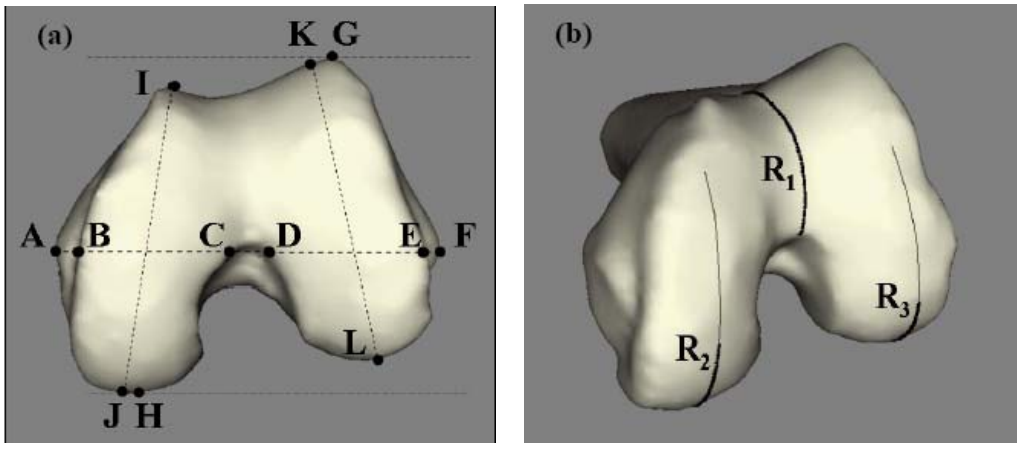

Figure 2.1: Illustration of commonly measured variables of the distal femur, listed in Table 2.1: (a) epicondylar width (AF), condylar width (BE), medial condylar width (BC), lateral condylar width (DE), overall AP (GH), medial AP (IJ) and lateral AP (KL); (b) patellofemoral radius (R1), medial posterior radius (R2) and lateral posterior radius (R3).

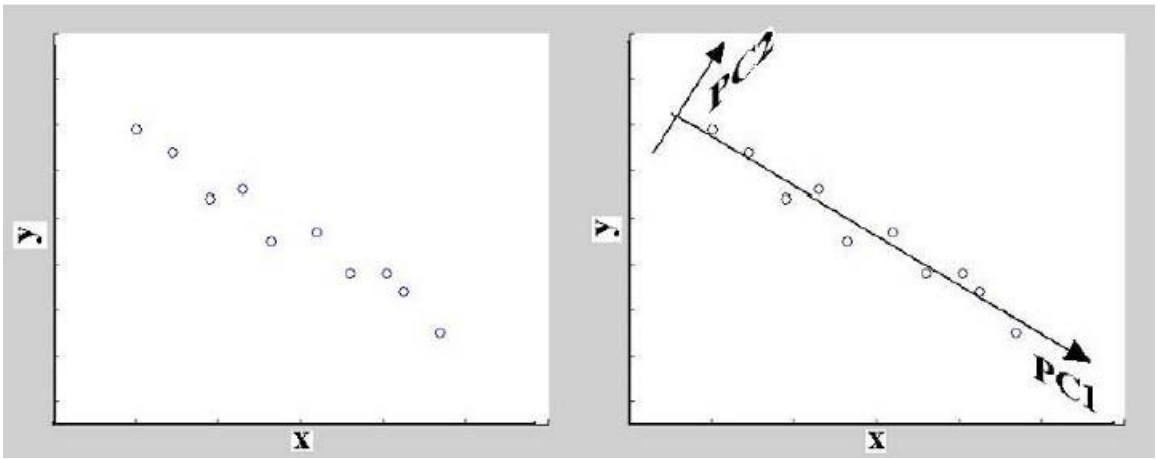

Figure 2.2: Left: Two variables x and y. Assumes y is dependent, and x is independent. Right: PC1 axis lies along the axis of maximum variation, with PC2 lying along the axis of maximum variation, subject to being orthogonal to PC1.

2.5 Tables

Table 2.1: Literature anthropometric data on the distal femur (male/female values separated by '/')

	Measurement Method	Ethnicity	n	Epicon. Width	Condylar Width	Medial Condylar Width
Mensch *et al*.	Cadaver	Caucasian	83	-	81.1/69.7	29.9/24.5
Yoshika *et al*.	Cadaver	Caucasian	32	90.0/80.0	83.0/72.0	32.0/27.0
Berger *et al*.	Cadaver	Caucasian	75	85.6/75.4	-	-
Walker *et al*.	Radiograph	Caucasian	50	-	-	-
Elias *et al*.	Radiograph	Caucasian	26	-	-	-
Mastuda *et al*.	MRI	Japanese	90	-	-	-
Rooney *et al*.	CT Scans	Caucasian	35	86.8/78.8	74.4/66.2	28.0/24.2
Rooney *et al*.	CT Scans	Japanese	79	85.8/73.8	74.1//62.2	28.9/24.6

	Lateral Condylar Width	Overall AP	Medial Condylar AP	Lateral Condyalr AP	Medial Posterior Radius	Lateral Posterior Radius	Patellofe moral Radius
Mensch *et al*.	31.4/26.6	-	68.1/61.2	67.9/61.9	-	-	-
Yoshika *et al*.	31.0/28.0	-	70.0/63.0	72.0/65.0	-	-	-
Berger *et al*.	-	-	-	-	-	-	-
Walker *et al*.	-	-	63.5/58.0	64.1/60.7			
Elias *et al*.	-	-	-	-	20.0	20.0	24.0
Mastuda *et al*.	-	-	-	-	20.3	19.0	-
Rooney *et al*.	31.4/28.7	76.1/69.5	69.0/62.5	69.8/63.8	21.0/19.1	22.2/19.8	22.1/21.1
Rooney *et al*.	32.0/27.4	72.4/64.7	28.9/24.6	65.5/58.8	20.6/17.9	19.8/17.9	19.8/18.9

Table 2.2: Correlation coefficients of various distal femoral measures for 187 subjects. 'Bold' numbers shows stronger correlation (Rooney *et al.*)

	Epiwd	AP	Conwd	Medcodwd	Latcondwd	Medcondap
Epiwd	1.00					
AP	**0.88**	1.00				
Conwd	**0.92**	**0.85**	1.00			
Medcodwd	0.63	0.56	0.70	1.00		
Latcondwd	**0.79**	0.75	**0.84**	0.58	1.00	
Medcondap	**0.86**	**0.95**	**0.83**	0.58	0.72	1.00
Latcondap	**0.86**	**0.95**	**0.82**	0.53	0.71	0.92
Trochlng	0.63	0.67	0.56	0.44	0.46	0.72
Trochwd	**0.89**	0.64	0.73	0.58	0.64	0.59
Patfemrad	0.55	0.59	0.46	0.42	0.39	0.67
Medpostrad	0.72	0.69	0.65	0.48	0.57	0.69
Latpostrad	0.70	0.71	0.66	0.41	0.59	0.70

	Latcondap	Trochlng	Trochwd	Patfemrad	Medpostrad	Latpostrad
Epiwd						
AP						
Conwd						
Medcodwd						
Latcondwd						
Medcondap						
Latcondap	1.00					
Trochlng	0.69	1.00				
Trochwd	0.55	0.34	1.00			
Patfemrad	0.63	0.74	0.28	1.00		
Medpostrad	0.70	0.58	0.43	0.53	1.00	
Latpostrad	0.73	0.54	0.41	0.48	0.74	1.00

Chapter 3: Development of a Statistical Model to Characterize Passive Envelope of Natural Knees

3.1 Introduction

The motion patterns of the human knee joint partially depend on a combination of its passive motion characteristics and the external loads. The former are described by the bony and the ligamentous constraints and the latter depends on muscle activity and external forces to the knee. The passive envelope of a knee is the overall laxity of the knee in any given degree-of-freedom throughout the flexion range. It is believed that the active motions like walking and squatting are influenced by the passive envelope, it is also thought that the passive motion characteristics of a knee could assist in understanding the knee joint kinematics [2, 3]. Although several authors have studied passive knee envelope characteristics, it is not clear from the literature which anatomical structures guide the knee in passive or active motion and how their geometric arrangement produces the unique path of passive knee motion [1-3, 28, 57]. A few mathematical models were developed to study the structures that guide the passive knee motion [1, 2]; however, the results obtained were highly sensitive to the ligament bundle description, its properties, and their intra-subject variability to ligament insertion-origin sites. To explain the relationship between knee anatomy and its variability with three-dimensional knee motion completely, variability in the kinematic envelope of a knee must be understood thoroughly.

Ligament balancing is an accepted and practiced step during total knee arthroplasty. Research has indicated that poor ligament balancing can contribute to failure through increased wear rates, implant loosening and abnormal kinematics [20, 25, 37]. To ensure

proper ligament balancing, almost all surgeons check knee laxity envelope at full extension and at multiple flexion angles. The change in passive envelope of motion from the natural condition could be used to observe the altered constraint and stability achieved with a TKA. To establish a strong link between the post-surgery and pre-surgery knee envelope, passive envelope of a native knee must be explored. The objective of the present study was to characterize the tibiofemoral passive envelope using a multivariate analysis technique, principal component analysis. The study tested the following hypotheses:

1. The maximum variation in the tibiofemoral passive envelope will be observed in its relative position throughout the flexion range.
2. Due to the taut ligaments, the minimum variation in V-V and I-E envelopes will be observed at full extension and early flexion (<20°). Whereas, due to the natural roll back and more consistent patterns in A-P motion, variation in the A-P envelope will be a minimum at deeper flexion (>100°).

3.2 Materials and Methods

Twenty-one fresh frozen cadaver legs (age: 63.7±10.9, BMI: 26.1±3.4) were thawed at room temperature and then dissected. For each leg, the femur and tibia were sectioned 28 cm proximal and 18 cm distal to the epicondylar axis. All soft tissue within 10 cm of the knee joint was left intact to prevent the dehydration of the tissue. Soft tissue more than 10 cm from the epicondylar axis was removed, with the exception of the multiple heads of the quadriceps tendons. Remainders of the tibia and femur were cleaned and cemented into tubular fixtures aligned parallel to the bones' intermedulary canals. A fixture was permanently mounted on the femoral tube, which was fixed on the surgical

table for the envelope assessment (Fig. 3.1). For the passive envelope of motion, the femur was fixed leaving the tibia to move freely. An assessment was performed manually by moving the tibia though the flexion-extension (F-E) range of motion (ROM) from full extension to full flexion. During the F-E ROM, loads and torques were applied until the tibial varus-valgus (V-V), internal-external (I-E) and anterior-posterior (A-P) motion was constrained. The constraint was felt by the researcher's tactile sensations and may not be a clear end point of that motion. Care was taken while applying the loads in order to avoid damaging the soft tissue around the joint.

Tibiofemoral motions were captured during the assessments by tracking rigid arrays of infrared-light emitting diodes mounted to the tibial and femoral fixtures using an Optotrak 3020 camera system (NDI, Waterloo, Canada). Reported accuracy of the system is 0.5 mm and 0.5º [58]. Several anatomical landmarks were identified and their locations were captured using a digital stylus. Probed anatomical points are listed in Table 3.1. Tibiofemoral kinematics were estimated using a modified Grood and Suntay knee kinematics description [59]. The V-V, I-E and A-P passive envelopes of a representative knee are given in Fig. 3.2. Achieved envelope boundaries were identified at each 1º of flexion angle (red and black dots in Fig. 3.2). Kinematic analyses were concentrated on the tibial V-V, I-E and A-P envelope boundaries as a function of knee flexion. The mid-point of envelope boundaries at full extension was subtracted from the rest of the envelope boundaries. This offseted data helped focus on envelope shape and size variability. The data was used for the further analyses.

Principal component analysis is a mathematical method of transforming a multivariate data set into a new set of variables called principal components, where each

of the PCs are linearly independent of one another [48]. The first few PCs can be used to explain the maximum variation in the original dataset. The more substantial the correlations among the original set of variables, the more variation will be explained by first few PCs. The detailed mathematical description of PCA is provided by Joliffe [48].

Separate PC models for V-V, I-E and A-P kinematics were developed. The data matrix consisted of **N** subjects (**N**=21), with **n** variables defining kinematics ($\boldsymbol{n}$ = 30). Kinematic variables were maximum and minimum point of an envelope at each 10º of flexion angle (0º-140º). Hence each subject $\boldsymbol{x_i}$ ($\boldsymbol{i}$ = 1, 2, …, $\boldsymbol{N}$) was represented by $\boldsymbol{n}$ kinematic variables. Let $\boldsymbol{D}$ be the $\boldsymbol{N}\times\boldsymbol{n}$ matrix, each column holding the variables for one subject. A $\boldsymbol{n}\times\boldsymbol{n}$ covariance matrix $\boldsymbol{C}$ was constructed with entry $\boldsymbol{C_{a,b}}$ containing the covariance between row $\boldsymbol{a}$ and row $\boldsymbol{b}$ of matrix $\boldsymbol{D}$. The eigenvectors and corresponding eigenvalues of matrix $\boldsymbol{C}$ were estimated. Each column of matrix $\boldsymbol{E}$, the eigenvector matrix, held an eigenvector $\boldsymbol{e_j}$ ($\boldsymbol{j}$ = 1, 2, …, $\boldsymbol{n}$) of matrix $\boldsymbol{C}$. The eigenvectors of $\boldsymbol{C}$ were the PCs of the data. The mean of each variable was calculated and stored in $1\times\boldsymbol{n}$ row vector $\boldsymbol{V_{mean}}$. The PC scores were calculated as the dot product of the PC and the variables. Let $\boldsymbol{P_{mean}}$ be $1\times\boldsymbol{n}$ column vector containing the PC scores of the mean variables. Thus,

$$\boldsymbol{V_{mean}}\boldsymbol{.E} = \boldsymbol{P_{mean}} \qquad \text{(Eq 3.1)}$$

The PC scores $\boldsymbol{P_{mean}}$ can be altered and the corresponding deformation V of the input kinematic and geometric variables can be calculated and displayed according to:

$$\boldsymbol{V = P.\ E^{-1}} \qquad \text{(Eq 3.2)}$$

where $\boldsymbol{E.\ E^{-1} = I_n}$, the identity matrix.

The range though which the PC scores could be altered was limited to ± 3σ, so that the only realistic effects of envelope boundaries on the envelope can be visualized.

PC model results included the PCs and the variance explained by them. Models were further deformed (within ±3σ) along each PC axis with all other PCs fixed at the mean, to identify the variation associated with that specific PC [12, 29]. Envelope factors associated with the first PC would be responsible for the corresponding change in the passive envelope. This PC interpretation process was continued until 90% of the variation in the input data matrix was explained.

3.3 Results

Envelope PCA models were carried out on each kinematic separately to investigate intra-subject modes of variation in the tibiofemoral envelope with the results shown in Table 3.2. Deformation of the model for the first two PC axes is displayed in Figures 3.3 through 3.5. Each figure represents the mean and ±3σ deformation along each PC axis. This method was used to interpret the variation explained by PCs. One should remember that the variation associated with each PC is an interpretation of that PC; the trends observed in the dataset without their quantification.

In the V-V envelope the first four PCs accounted for 96.9% of the total variation. PC1, explaining almost 78% of variation, which was observed due to the change in relative position of the envelope (Fig. 3.3 a). PC2 (12.2%) captured the varying size of envelope without changing its relative position (Fig. 3.2 b). PC3 (3.9%) explained the variation in the relative position of envelope at early flexion (<40º). A small amount of variation was observed in the V-V envelope size during 30º-90º of flexion, which was captured by the PC4.

In the I-E envelope, four PCs accounted for 90% of the variation. Similar to V-V envelope, the first PC (62.9%) explained the variability in the relative position of the envelope (Fig. 3.4 a). Second PC (15.1%) accounted for the envelope size (Fig. 3.4 b). Interpretation of PC3 provided few interesting results. Small variation was observed in the envelope relative position at early flexion (<40º), whereas, variability in the envelope size during mid-flexion (30º-90º) was also noticed. These subtle but important differences were captured by PC3 (7.7%) and PC4 (4.9%) respectively. For A-P envelope, the first PC (78.6%) accounted for the relative position of the envelope, while the second PC (7.8%) captured the variation in the envelope size. Variation in the relative position of an envelope at later flexion (>40º) was accounted by PC3 (5.3%), whereas, varying envelope size during 30º-90º flexion was characterized by PC4 (2.8%).

3.4 Discussion

The PC modeling provides a huge potential to interpret and understand the multivariate knee kinematic datasets. Several authors have demonstrated the usefulness of PCA in knee biomechanics to reduce the dimensionality and explain inter-subject variability during various loading profiles like gait waveforms [49, 50, 60], sit-to-stand profiles [51], and lifting waveforms [61]. Despite the wide range of applications, almost no study in the literature addresses the use of PCA to interpret passive knee envelope and variation associated with it. PCA models developed in this study not only interpret the envelope variability but also identified the subtle modes of variations which are usually overlooked by the other data analysis strategies.

To test Hypothesis 1 that the relative position of the envelope is the major mode of the variation, PCA models of tibiofemoral envelopes were developed. For all three

kinematic envelopes, almost three-fourths of the variation was captured by the first PC and caused due to the relative position of the envelope (Table 3.1). Several researchers experienced intra-subject variability in their *in vivo* and *in vitro* envelope assessment studies. Walker *et al*. [6] found from their *in vitro* experiment that the rotary (V-V and I-E) and translational (A-P) laxities were as much as four times from one specimen to another. Although the group associated the phenomenon with the experimental procedure, researchers suggested that knee laxity depends strongly on the individual subject. O'Connor *et al*. [62] tested twelve cadaveric specimens to identify passive envelope and passive path of flexion. There were no consistent patterns of I-E, V-V and A-P envelopes. Similar results were observed by Blankevoort *et al*. [3] and Andriacchi *et al*. [47] in their respective *in vitro* studies.

Overall laxity patterns observed in this study were consistent with the previous research [3, 22]. The knees were tight at full extension for V-V, I-E and A-P motions. The overall ROM or envelope size increased until 30º flexion, after which it remained relatively consistent with increasing flexion angle. At deeper flexion (>120º), again envelope size shrank for all three motions (Fig. 3.2). Variability in the envelope size was captured by the second PC (Table 3.1). Similar to the relative position of an envelope, envelope size could be highly specimen dependant. In another *in vitro* study of four cadavers Blankevoort *et al*. [3] observed that the shape of rotational laxity vs. flexion angle curves was similar among different specimens but with the consistent shift in the magnitudes, indicating envelope size variation across knees. Unlike rotational laxities,

A-P laxity is not considered as a degree of freedom-of-motion. In a strict sense it implies whether a noticeable resistance to A-P force is present or not. Therefore, varying envelope size of A-P motion could be considered as a varying resistance to the A-P force.

Numerous studies investigating an overall knee size concluded that the femoral width could be used to define a knee size [11, 17]. Also, stronger correlations between femoral width and cruciates size [8], collaterals size and tibial and patellar bone sizes [8, 11] have been established. Cadavers tested in the current study were diverse in their size (BMI: 20.1-30.0, weight: 60.1-100.0 kg, knee size: 80.5-92.8 mm). Moreover, considering the intra-specimen variability in the tested cadavers, variation observed in the current study is not surprising; however, PCA was able to sub-categorized and quantify the mode of maximum variation (PC1~75%, PC2~15%) and interpret it accordingly (relative position of an envelope and envelope size).

Variance explained by the subsequent PCs was relatively small (PC3~5%, PC4~3%); however, they characterized interesting envelope behaviors. For V-V and I-E laxities, PC3 highlighted the variation in the envelope position at early flexion angles (<40º). It has been observed previously that at full extension cruciate ligament bundles, posterior capsule and LCL are loaded and taut [1, 13, 63]. However, passive flexion of the knee from 0º-40º caused the antero-medial and postero-lateral aspects of the ACL, along with the posterior element of the PCL to decrease in length and become slack or unloaded. The change was also accompanied by the slack lateral aspects of joint capsule, allowing external tibial rotation with flexion [1]. This ligament loading phenomenon combined with the variation in the ligament size, its stiffness and origin-insertion site may be responsible for the varying relative position of the envelope at early flexion. For all three

motions, PC4 captured the variation in the envelope size during mid-flexion. Few mathematical and computational models observed taut antero-medial ACL and PCL and the recruitment of collateral ligaments and capsular structures during mid-flexion (30º - 100º) [1, 30]. The variation in envelope size could be a result of the interaction between ligaments and tibiofemoral joint kinematics during mid-flexion. Although these inferences provide important information about the passive knee envelope, these hypotheses are not tested specifically. Future investigation is necessary to find which anatomical structures guide the knee in passive flexion and how their geometric arrangement produces the unique path of passive knee envelope.

The PC modeling approach for the native passive knee envelope can later be used to compare the post-surgery envelope characteristics. The current experiment has several limitations. Envelope boundaries (motion constraints) were obtained solely by the tactile sensation experienced by the researchers. This raises the concerns about the accuracy and the reproducibility of the envelope boundaries. Also, cadaveric tissue degradation throughout the experimental protocol was a major concern; however, skin and other musculature surrounding the joint were left intact and saline water was frequently applied to avoid dehydration of the tissue. Another drawback of the experimental setup was the absence of any static or dynamic loading on the muscles. Several studies have demonstrated the effects of illiotibial band, hamstring muscles and quadriceps muscles on the active and passive stability of a knee joint. Therefore one has to be careful while comparing results with the results obtained from *in vivo* studies. However, the results provide a platform for understanding the roles of specific anatomical or geometrical factors on the knee kinematics during passive or active motions. Future models are

required to identify the anatomical factors responsible for the passive or active knee motion.

This study demonstrated the capability of PCA and its application to identify modes of variation in the passive knee envelope. Envelope PC models highlighted the variability in the relative position of envelopes with the first PC, whereas the envelope size was generally captured by the second PC. Subsequent PCs divided the flexion range into two distinct regions and highlighted the envelope variation occurring in those regions. The modeling methodology will be further developed to understand the variation in active motion paths like gait and squat of native knees. The technique will be useful to interpret the effects of various surgical changes, implant alignment, implant size etc., on knee kinematics or its envelope.

3.5 Figures

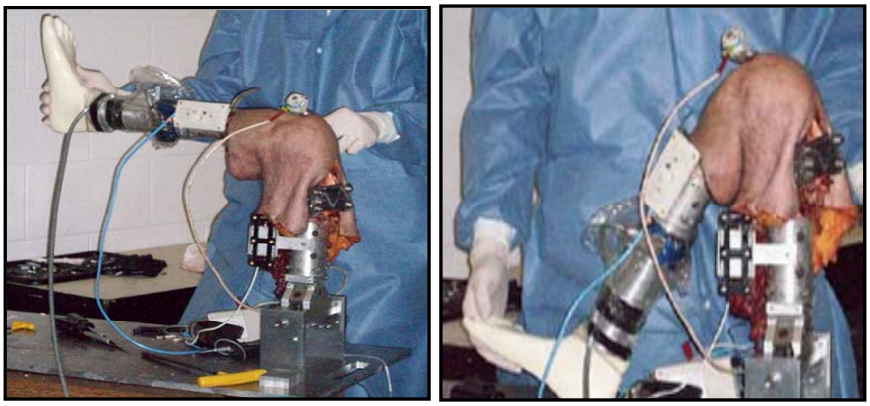

Figure 3.1: Experimental setup for the tibiofemoral passive envelope of motion assessment, femur is fixed and tibia is free to move. During F-E ROM torques and loads were applied manually until tibial V-V, A-P and I-E motions were constrained

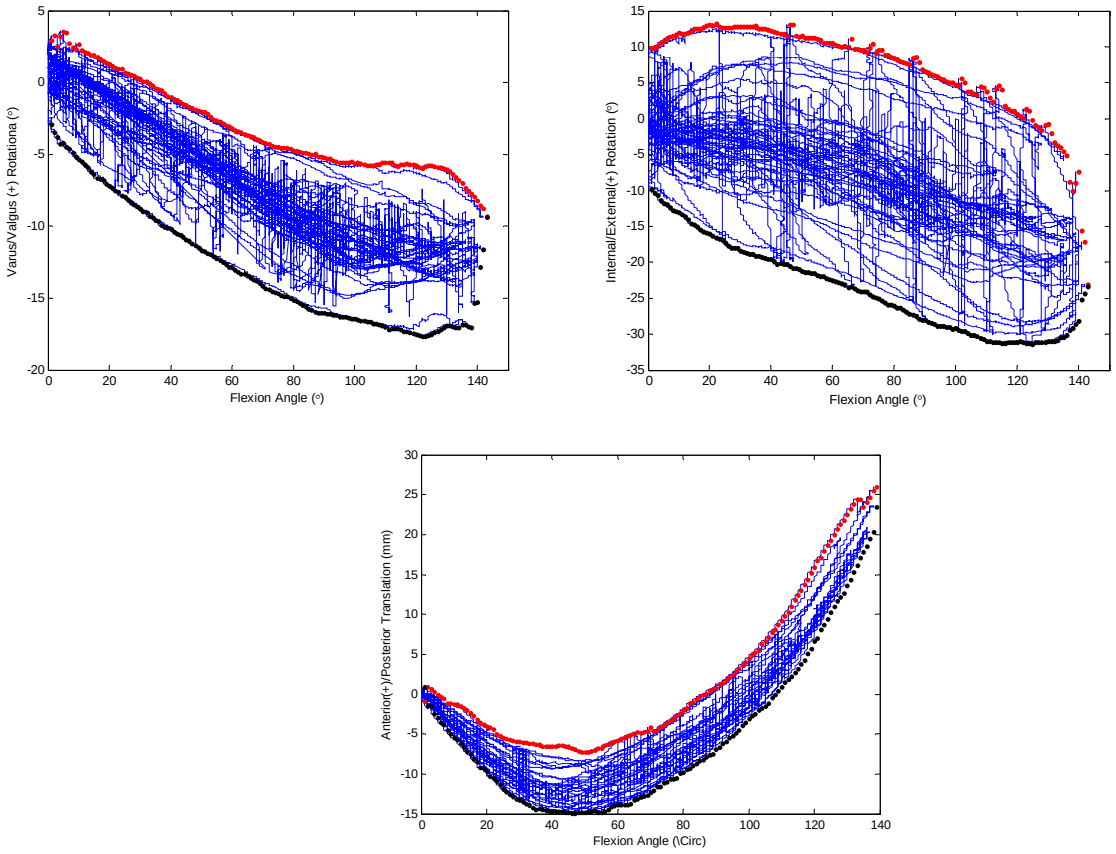

Figure 3.2: Raw experimental kinematics data (blue) of V-V, I-E and A-P envelope of motion as a function of knee flexion angle. Boundaries of envelope at each flexion angle are identified (red and black) and were used for developing PC model. The data presented is from a representative knee.

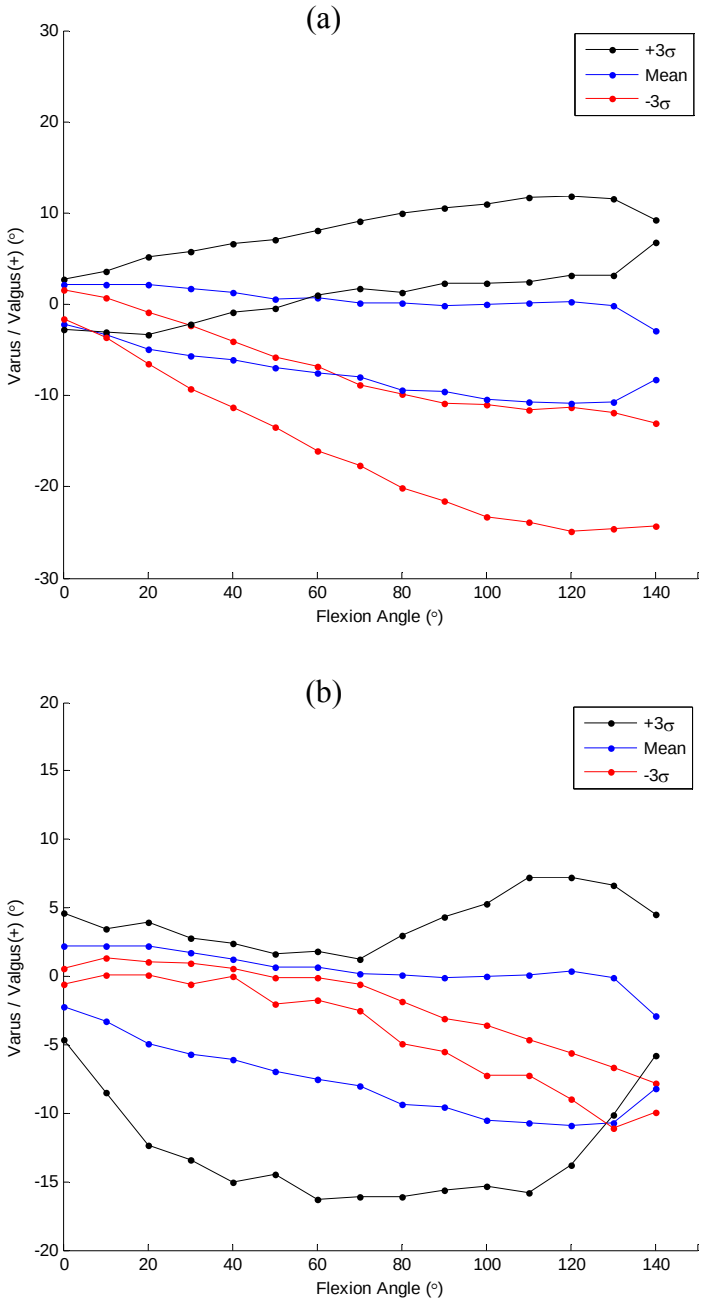

Figure 3.3: -3σ, mean and +3σ deformation along (a) PC1 (78.2%) and (b) PC2 (12.5%) axis for the V-V envelopes as a function of flexion angle. Blue lines are the average envelope boundaries of all knees (N=21) at each flexion angle. Black lines shows the envelope boundaries at +3σ, whereas red lines represents the envelope boundaries at -3σ obtained by deforming model at the specific PC axis while all other PCs were fixed to mean

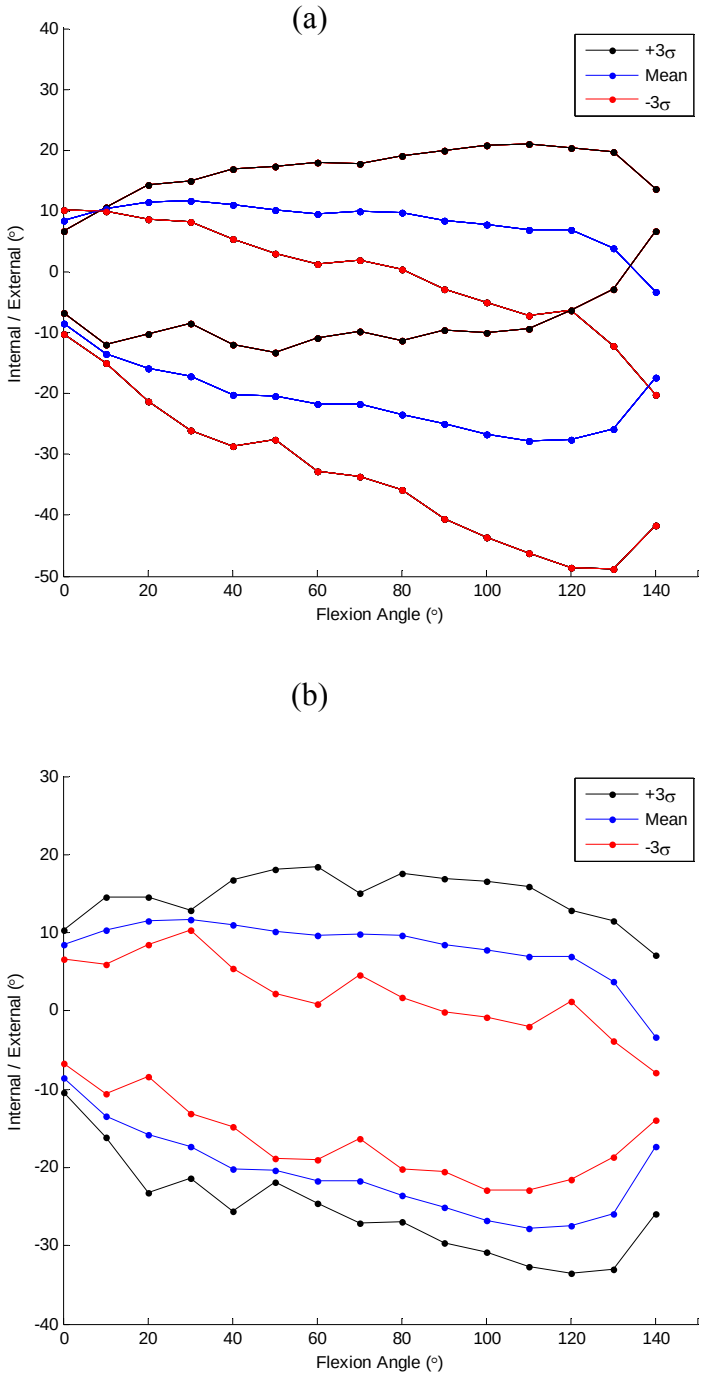

Figure 3.4: -3σ, mean and +3σ deformation along (a) PC1 (62.9%) and (b) PC2 (7.8%) axis for the I-E envelopes as a function of flexion angle. Blue lines are the average envelope boundaries of all knees (N=21) at each flexion angle. Black lines shows the envelope boundaries at +3σ, whereas red lines represents the envelope boundaries at -3σ obtained by deforming model at the specific PC axis while all other PCs were fixed to mean

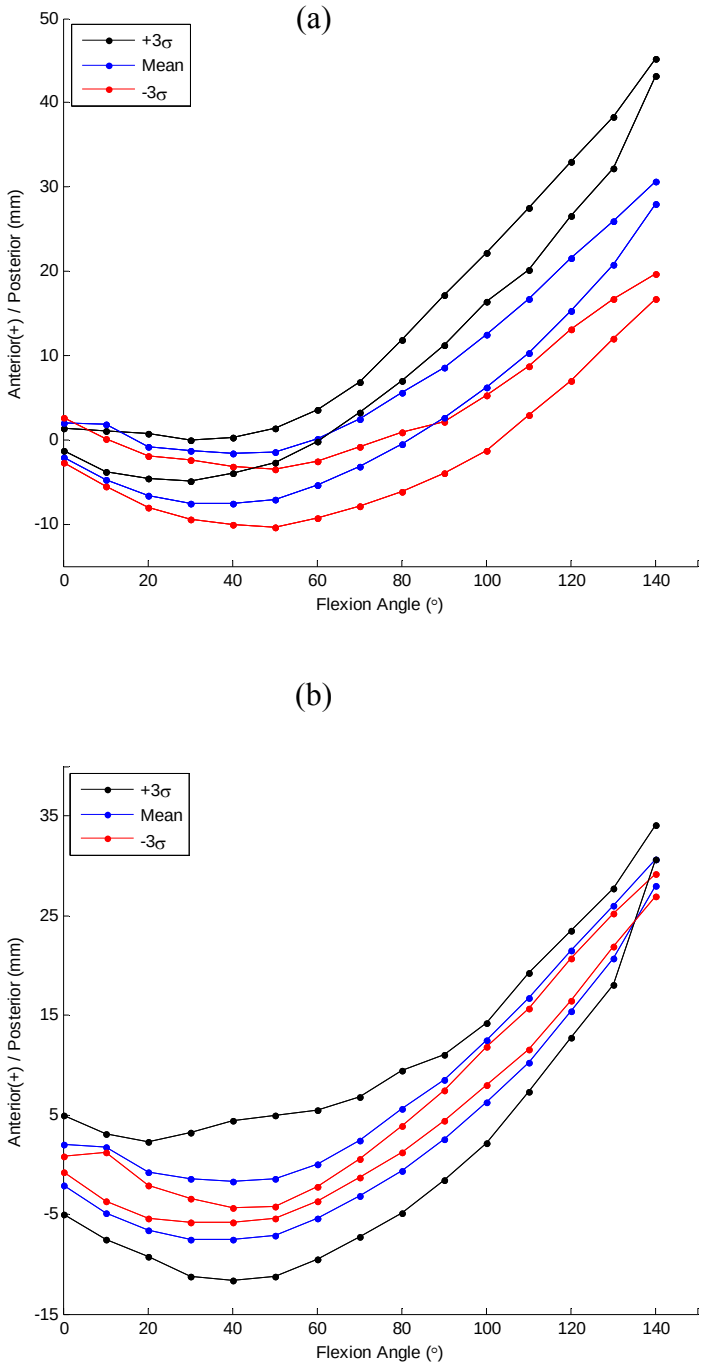

Figure 3.5: -3σ, mean and +3σ deformation along (a) PC1 (78.6%) and (b) PC2 (24.1%) axis for the A-P envelopes as a function of flexion angle. Blue lines are the average envelope boundaries of all knees (N=21) at each flexion angle. Black lines shows the envelope boundaries at +3σ, whereas red lines represents the envelope boundaries at -3σ obtained by deforming model at the specific PC axis while all other PCs were fixed to mean

3.6 Tables

Table 3.1: Anatomical points identified and probed to describe tibiofemoral kinematics in modified Grood and Suntay knee kinematics description [64]

No	Anatomical Landmark
1	Medial femoral posterior condyle
2	Lateral femoral posterior condyle
3	Most distal point on femoral groove
4	Center of femoral head
5	Medial tibial plateau
6	Lateral tibial plateau
7	Proximal tip of tibial eminence
8	Center of the bone canal at distal end of tibia

Table 3.2: The percent variation in data explained by the first four PCs for the Envelope PCA model of V-V, I-E and A-P envelope

Envelope	Variation %		Total Variation (%)	Interpretation
V-V	PC1	78.2	78.2	Relative position of Envelope
	PC2	12.5	90.7	Envelope Size
	PC3	3.9	94.6	Relative position of envelope at early flexion (<40°)
	PC4	2.3	96.9	Envelope Size during 30°-90º flexion
I-E	PC1	62.9	62.9	Relative position of Envelope
	PC2	15.1	78.0	Envelope Size
	PC3	7.7	85.7	Relative position of envelope at early flexion (<40°)
	PC4	4.9	90.6	Envelope Size during 30°-90º flexion
A-P	PC1	78.6	78.6	Relative position of Envelope
	PC2	7.8	86.4	Envelope Size
	PC3	5.3	91.7	Relative position of envelope at later flexion (>40°)
	PC4	2.8	94.5	Envelope Size during 30°-90º flexion

Chapter 4: Relationship between Knee Anatomy, Passive Envelope and Dynamically Simulated Gait: A Predictive Tool using Principal Components

4.1 Introduction

The ligaments play an important role in providing the passive stability of the joint, partially due to the relative incongruency of the articular surfaces. The passive motion characteristics of the human knee-joint is partly depend on the mechanical and structural interaction between the articular surfaces, the ligaments and other soft tissue structures. Several authors have studied the passive envelope characteristics of the knee; however, it is not clear from the literature how the variation in anatomical features influenced the kinematics during passive envelope or active motions and how the variation in their geometric arrangement produces the observed path during active motions [2-4, 19]. During dynamic activities like walk and squat, a critical interaction occurs between multiple muscle forces crossing the knee, compressive force at the joint and forces in the passive soft tissue. Researchers attempted to determine the interaction between passive and active laxity of the knee joint, though with limited success due to intra-subject variability and the computational model's sensitivity to numerous variables [17, 19]. This gives rise to the need to understand the role of anatomical features in guiding the passive envelope or active knee motions.

It is unclear how the articular geometry and muscle activations of the knee influence the contribution of ligament constraints during dynamic activities. Also, the relationship between the passive knee envelope and the kinematics during various dynamic activities has not been studied thoroughly. Schipplein *et al.* developed a simplified mathematical model of a knee to understand the contribution of active stabilizers, such as muscle forces, and passive stabilizers, such as soft tissues, during level gait [47]. The group concluded that the contribution of both active and

passive stabilizers was important in achieving dynamic knee stability during gait. Despite the meaningful results, group did not characterize contribution of muscle and ligament forces in guiding the knee motion due to the simplicity of the model. The tibiofemoral kinematics during active motions, like gait and squat, can be better understood by exploring their relationship with the passive knee envelope.

During total knee arthroplasty (TKA), surgeon follows several ligament balancing philosophies to achieve the best post-TKA knee performance. For varus or valgus deformity, it is often necessary to surgically release the collaterals on the concave side of the knee to restore equal flexion-extension gap [20, 65]. In his *in vivo* study, Engh *et al.* observed that patients with the valgus deformity had tight lateral collateral ligament (LCL), which was later released during TKA [20]. In their qualitative assessment, the group observed superior attachment of the LCL and associated it with the LCL tightness. Further understanding of relationship between soft tissue structures, their attachment locations and the functional kinematics can help offer surgeon more options for the intra-surgery ligament balancing.

Principal component analysis is a statistical tool used in the analysis of multivariate data. Several authors have used principal component analysis (PCA) in knee biomechanics to reduce the dimensionality and explain inter-subject variability of the gait waveform [11, 49, 66, 67]. Moreover, the technique has been widely accepted in the shape morphing algorithms, the modeling method used to obtain a complete surface model from sparse data sets [13, 55]. The method first uses a training dataset to estimate the mean shape of the surface. The modes of the variation, PCs, are found using PCA on the deviations of the training set from the mean. These modes or PCs are represented by orthogonal eigenvectors. A new shape is generated by adding linear combinations of the most significant variation vectors to the mean shape. Styner *et al*.

further modified a PCA-based morphing technique by operating directly in the PCA shape space by incorporating large sets of possible variations including both spatial and non- spatial information such as patient height, weight, age etc [68].

A principal component analysis for the knee can be used to understand the underlying variability in the anatomical features, its passive envelope, and joint kinematics during weight-bearing activities. Moreover, once the model is generated, a morphing scheme can be used to predict the tibiofemoral kinematics during various activities using anatomical features and a few envelope measures. In the prediction algorithm, like shape prediction, tibiofemoral kinematics will be considered as a shape to be predicted, whereas the anatomical and envelope measures will be treated as sparse data points. The primary objective of this research was to measure the correlation between the anatomical variation of the natural knee with observed tibiofemoral kinematics during a passive knee envelope and simulated dynamic activities using a knee simulator. A second objective was to identify the anatomical and envelope factors that explain the maximum variation in the tibiofemoral kinematics during gait and use them to predict knee kinematics using a PCA based morphing algorithm.

4.2 Materials and Methods

4.2.1 Experimental Setup

The seventeen fresh frozen cadaver legs (age: 64.3±10.3, BMI: 27.3±3.5) were thawed at room temperature and then dissected. For each leg, the femur and tibia were sectioned 28 cm proximal and 18 cm distal to the epicondylar axis. All soft tissue within 10 cm of the knee joint was left intact to prevent the dehydration of the tissue. Soft tissue more than 10 cm from the epicondylar axis was removed, with the exception of the multiple heads of the quadriceps tendons. Remainders of the tibia and femur were cleaned and cemented into tubular fixtures

aligned parallel to the bones' intermedulary canals. For the passive envelope of motion, the femur was fixed leaving the tibia to move freely (Fig. 5.1). An assessment was performed manually by moving the tibia though the flexion-extension (F-E) range of motion (ROM) from full extension to full flexion. During the F-E ROM, loads and torques were applied until the tibial varus-valgus (V-V) and internal-extenral (I-E) motion was constrained. The constraint was felt by the researcher's tactile sensations and may not be a clear end point of that motion. Care was taken while applying the loads in order to avoid damaging the soft tissue around the joint.

After the envelope assessment, the knee underwent a dynamically simulated gait cycle in the Kansas Knee Simulator (KKS) (Fig. 4.2) [69]. The Kansas Knee Simulator has five axes of control: 1) a vertical load at the hip, 2) a quadriceps load, 3) a torque about a vertical axis through the ankle, 4) a medial-lateral ankle force, and 5) an ankle flexion moment. The knees underwent simulated walking using 50% bodyweight derived from an ISO standard [46]. Knees were aligned in the KKS during squatting to maintain a vertical orientation of the tibia and minimize tibial I-E rotation and mediolateral (M-L) translation of the ankle. The alignment adjustments included V-V angle and I-E rotation of the femur relative to the hip and I-E rotation of the tibia relative to the ankle. The quadriceps actuator could translate and rotate in the frontal plane and was aligned with long axis of the femur and the center of the patella.

During all assessments, tibiofemoral motions were captured during the assessments by tracking rigid arrays of infrared-light emitting diodes mounted to the tibial and femoral fixtures using an Optotrak 3020 camera system (NDI, Waterloo, Canada). Reported accuracy of the system is 0.5 mm and 0.5º [58]. Several anatomical landmarks were identified and their locations were captured using a digital stylus. Tibiofemoral kinematics were estimated using a modified Grood and Suntay knee kinematics description [59].

4.2.2 Obtaining Anatomical Variables

After testing, the knees were dissected down to the joint capsule and locations of the medial and lateral collateral ligaments and medial and lateral epicondylar axis (EpA) were recorded using a digital stylus. Series of points were collected at the collateral's origin sites and the centroid of these points was used for the analysis. Subsequently, the Cartesian coordinates of these points were described in the femoral Grood and Suntay coordinate frame. Using medial and lateral epicondylar points the epicondylar width (EpW) was calculated. Also, the orientation of epicondylar axis in femoral anatomical coordinate frame was estimated. Orientation of epicondylar axis in frontal and transverse plane was referred as frontal plane angle (FPA) and transverse plane angle (TPA) respectively.

4.2.3 PCA Model Development

The aim of a PCA is to reduce the dimensionality of a multivariate dataset while retaining as much variation as possible. The PC model that was created separates and quantifies the major variation in the data that occurs within the population of the cadaver passive envelopes and gait kinematic data. PCA defines a linear transformation that decorrelates the parameter signals of the original data by projecting the objects into a linear data space spanned by a complete set of orthogonal basis vectors (PCs). If the variables are highly correlated, then the major variations in the dataset are described by the first few basic vectors.

A separate PC model was developed for the V-V and I-E rotations. Achieved envelope boundaries were identified at each 1º of knee flexion angle and kinematics at each 1% of the gait cycle. The data matrix consisted of $\boldsymbol{N}$ cadavers ($\boldsymbol{N}$=17), with $\boldsymbol{n}$ variables defining anatomical, envelope and gait kinematics variables. Cartesian coordinates of the medial and lateral epicondylar point, and origins of medial and lateral collateral ligaments along with EpW, FPA

and TPA described anatomical variables (n_1=15). Envelope variables were achieved maximum and minimum point of the envelope at each 1º of flexion angle (0º-130º, n_2=262), whereas, gait variables were tibiofemoral kinematics at each 1% of gait cycle (n_3=101). Hence each cadaver x_i (i = 1, 2, …, N) was represented by n (n= n_1+ n_{2+} n_3) data variables. Let P be the $N \times n$ matrix, each column holding the variables for one subject. Since the input matrix contains variables with different units, a normalized *z*-score matrix was estimated, which was used for subsequent calculations. After PCA, the *z-score* matrix was transformed back to the original basis. A $n \times n$ covariance matrix C was constructed with entry $C_{a,b}$ containing the covariance between row a and row b of matrix P. The eigenvectors and corresponding eigenvalues of matrix C were estimated. Each column of matrix E, the eigenvector matrix, held an eigenvector e_l (l = 1, 2, …, n) of matrix C. The eigenvectors of C were the PCs of the data. The mean of each variable was calculated and stored in $1 \times n$ row vector V_{mean}. The PC scores were calculated as the dot product of the PC and the variables. Let P_{mean} be $1 \times n$ column vector containing the PC scores of the mean variables. Thus,

$$V_{mean} . E = P_{mean} \qquad \text{(Eq 1)}$$

The PC scores P_{mean} can be altered and the corresponding deformation V of the input kinematic and geometric variables can be calculated and displayed according to:

$$V = P . E^{-1} \qquad \text{(Eq 2)}$$

Where, $E.E^{-1} = I_n$, the identity matrix.

The range though which the PC scores could be altered was limited to ± three standard deviations so that the only realistic effects of envelope boundaries on the envelope can be visualized.

PC model results included the PCs and the variance explained by them. The model was further deformed (within ±3σ) along each PC axis with all other PCs fixed at the mean, to identify the variation associated with that specific PC. Envelope or anatomical factors associated with the first PC would be coupled with the corresponding change in the envelope and gait kinematics. If anatomical factors changed more than ±50% from its mean value, it was considered to be the factor coupled to the corresponding change in the envelope and gait kinematics. The PC interpretation process was continued until 90% of the variation in the input data matrix was explained. One should remember that the variation associated with each PC is an interpretation of that PC; the trends observed in the dataset without their quantification.

4.2.4 Kinematics prediction from envelope measures using PCA model

Styner *et al.* developed a novel bone morphing scheme operating directly in the PCA shape space, incorporating a large set of possible variations including additional parameters such as patient height, weight, age, etc.[68] The method is based on the iterative removal of shape information associated with the digitized points. First, the most probable shape subject to the boundary conditions that are related to the initially digitized landmark was calculated. The resulting outline was used for registration and as an initial configuration for computing the most probable shape for the next digitized point. Using statistical shape analysis, the remaining shape variability was examined, after the surface information coded by the digitized points is progressively subtracted. This procedure of point selection and variability removal was repeated until a close approximation to the patient anatomy was achieved. The final extrapolated surface represented the most probable surface in the shape space given the digitized landmarks. The mathematical algorithm is described in Appendix A.

Proposed prediction model operates in the eigenvector space and can handle both spatial and non-spatial datasets. Predictions were performed using all anatomical variables and minimum and maximum boundaries of the envelope at 10°, 50° and 100° of knee flexion. Selected anatomical and envelope measures, considered as shape landmarks, were used to obtain the entire envelope and gait kinematics, considered as a complete shape, by calculating the most probable shape subjected to the boundary condition described by the anatomical and envelope measures.

The leave-one-out analysis was carried out to evaluate the accuracy and reproducibility of the prediction algorithm. For I-E and V-V kinematics, entire envelope and tibiofemoral kinematics during gait were predicted using anatomical features and the envelope boundaries at 10°, 50° and 100° of knee flexion. Each of these angles were considered as a representative flexion angle during stance and swing phases of the gait. The RMS error between predicted and experimentally collected envelope and kinematics was calculated for each prediction. The magnitude of the RMS error would be used to evaluate the accuracy and precision of the morphing algorithm.

4.3 Results

4.3.1 V-V PCA Model

Results of V-V motion with anatomical and envelope features are summarized in Table 4.1. Three PCs explained 92.0% variation in the V-V dataset. PC1 captured variation in the relative position of the envelope and gait, explaining 49.0% of the variation (Fig. 4.3). The change was also coupled with the FPA and S-I location of EpA and LCL. Deformation along the PC1 axis showed that the valgus shift in the envelope was coupled with the valgus shift in gait (Fig. 4.3). This valgus shift was observed with the superior location of LCL and EpA, which essentially

increased the FPA. The varus shift of an envelope showed varus shift of gait and inferior location of LCL and EpA with reduced FPA.

PC2 captured 35.2% of the variation summarizing a varying size of the envelope and range of motion during gait. PC2 also explained the variation in the EpW and the M-L location of MCL and LCL origin (Fig 4.3). Deformation along PC2 axis demonstrated that the increase in envelope size was coupled with the increase in the range of motion during gait (Fig. 4.3). Furthermore, the change was coupled with larger EpW and the M-L locations of the both collaterals. The origin of the MCL shifted medially, whereas LCL origin shifted laterally. Although the variance explained by PC3 was low, meaningful information was summarized by them (Table 4.1).

4.3.2 I-E PCA Model

Three PCs explained about 91.3% of the variation in the I-E dataset. The first PC captured variation in the relative position of the envelope and gait, explaining 51.8% of the variation (Table 4.1). The change was coupled with the varying TPA and A-P location of EpA and both collaterals. When the PC1 was deformed between $\pm 3\sigma$, externally shifted envelope was observed with the externally shifted gait waveform (Fig. 4.3). The change was coupled with the increasing TPA, due to the posterior shift of the lateral EpA and LCL origin with the anterior shift of the MCL origin. PC2 captured 24.7% variation in the dataset and was due to the varying sizes of the envelope and gait range of motion. The variation was observed with the EpW and the M-L locations of the both collaterals. Deformation along the PC2 axis showed that the increase in EpW occurred with the increase in the envelope size and I-E range of motion during gait. Also, the medial epicondylar point and origin of the MCL shifted medially, whereas, the lateral epicondylar point and LCL origin shifted laterally.

4.3.3 Kinematics Prediction and Model Validation

Leave-one-out analysis was carried out to estimate and compare the predicted outcomes. The PCA model was built using sixteen samples to predict the envelope and kinematics of the left-out sample. The V-V (Fig. 4.3) and I-E (Fig. 4.4) envelope and gait kinematics using a few envelope measures (envelope boundaries at 10°, 50° and 90° flexion) and anatomical features was predicted. For V-V model, RMS error for the envelope and gait kinematics was 0.5° and 1.2° respectively (Fig. 4.3). Whereas, for I-E model, RMS error for the envelope and gait kinematics was 0.7° and 0.8° respectively (Fig. 4.4). In order to estimate the reproducibility of the prediction, envelope and gait kinematics of each knee was predicted and the RMS error for both V-V and I-E envelope and gait was estimated (Table 4.2).

4.4 Discussion

Further understanding of relationship between the knee passive envelope and the kinematics during various dynamic activities can shed light on the role passive structures play in stabilizing knee joint. Results summarized here provided an insight into the relationship between a few anatomical factors, and the observed envelope and gait kinematics. Furthermore, results also highlighted the relationship between passive knee envelope and functional kinematics during gait. The study demonstrated the capabilities of PCA not only as an important statistical technique for analyzing multivariate data but also as a predictive tool.

A number of researchers have developed PC models to understand the basic variability in the knee kinematics dataset [49, 54, 66]. A few of them further developed their models to identify the individual motion patterns by extracting principal modes of variation of the dataset [50, 52]. However, PCA has been widely used in shape modeling to summarize the variability in the bone shapes and further predict the entire shape using a few surface points; the process is widely

known as a bone morphing [12, 55, 70]. Bryan *et al.* developed a PC model using forty-six femurs to predict the meshed-femur bone with its mechanical properties [70]. Styner *et al.* developed another PCA based algorithm to predict the bone shapes using both spatial, such as Cartesian coordinates of nodes, and non-spatial variables, such as age, height, weight, etc. [68]. The schemes proposed by Styner *et al.*, which was used in this study, is novel in that it operates directly in PCA shape space and incorporates the full set of possible variations including non-spatial parameters.

The PC model developed here summarized the baseline variation in the envelope, gait kinematics and the anatomical factors. Deformation along each PC axis demonstrated the influence of individual variables on one another. For both V-V and I-E motions, PC1 summarized variation in the relative position of the envelope and gait (Fig. 4.3 and 4.4). The change was coupled with the frontal and transverse plane alignment of EpA. Results indicated that the change in the EpA orientation in respective plane affected the tibiofemoral motion occurring in that plane. Furthermore, location of MCL and LCL origin changed in the direction of the orientation of EpA, indicating that the collateral origins are closely associated with the location of EpA. The finding is important and can help interpret surgical technique used for the femoral implant alignment. Usually, surgeons decide V-V alignment of the femoral implant using medial and lateral epicondyle [71, 72]. In their qualitative assessment, Insall *et al*. reported that such an alignment ensures location of epicondylar points and collateral origins close to the flexion-facet-center, the center of the posterior femoral codyles [73]. The results obtained in this study quantified the observation made by Insall *et al.* that both EpA and collateral origins stay in close proximity of each other. In another pre-surgery qualitative assessment of TKA patients, Engh *et al* observed that the patients with valgus deformity had superior LCL attachment and

also demonstrated valgus shift in the passive knee envelope [20]. In these patients, lateral epicondylar was relatively superior and close to the LCL origin. The group provided these trends without any quantification; however, results observed in the current study are in agreement with the trends reported by Engh *et al*.

PC2 summarized the envelope size and the range of motion during gait for both V-V and I-E kinematics. It can be inferred that the increase in the EpW was associated with the larger envelopes, which was related to the range of motion during gait. Recent morphological studies have concentrated on identifying EpW as one femoral dimension to represent the size of an entire knee. While studying the resection surface geometry of a knee, Fitzpatrick *et al*. found a positive correlation between femoral epicondylar width and tibial size variables [11]. Similar results were found by Mahfouz *et al.*[12], Lavellee *et al.* [12] and Rooney *et al.*[8] in their *in vivo* studies. Rooney *et al*. observed that the EpW was positively correlated with the A-P width, condylar width and radii of both medial and lateral femoral condyles. Also, stronger correlations between femoral width and cruciates size [8], collaterals size and tibial and patellar bone sizes [8, 11] have been established. These anatomical features may have played a role in the observed size changes in the envelope and gait kinematics.

During stance phase of a gait cycle, compressive loads at a knee joint can reach up to three times bodyweight [35, 46]. Under such a high compressive load and quadriceps force, tibiofemoral stability is achieved by the dynamic knee stabilizers; however, ligaments and other soft tissue structures play an important role in restricting joint motion. The passive envelope of motion characterizes effects of these soft tissue structures. During the swing phase of gait, there is limited compressive loading across a knee joint and the tibiofemoral motion is a passive motion, which is partially driven by the passive knee structures. Therefore, in both the stance and

swing phases of gait, passive knee stabilizers plays an important role, which was quantified by the PCA model developed here.

This study not only helps understand the interaction between knee anatomy, passive envelope and functional kinematics, but also presents the predictions algorithm for envelope and kinematics using a few anatomical and envelope factors. A PCA based bone morphing algorithm uses a few landmarks to predict the entire bone shape. Selective anatomical and envelope factors, considered as shape landmarks, were used to obtain the entire envelope and gait kinematics, considered as a complete shape, by calculating the most probable dataset subjected to the boundary condition described by the anatomical and envelope variables. Previous studies have shown larger patient-to-patient variation in the mechanical properties of the soft tissue structures [3, 45]. This variation affects the predictions made by the computational models, which uses the mechanical properties of knee soft tissue. In the current study, predictions were made accurately and precisely using the statistical approach. During TKA, surgeons do not have a priori knowledge about the patient's kinematics. Besides MRI, surgeons usually use the pre-surgery passive knee envelope assessment to gain more understanding about the patient's kinematics. Surgeons could use these assessments and obtain a-priori information, anatomical and envelope features, which could be later used to predict patient-specific envelope and kinematics during functional activity such as gait.

For envelope factors, achieved minimum and maximum envelope boundaries at 10°, 50° and 100° knee flexion were obtained. Each of these flexion angles are representative of the range of flexion angles during stance and swing phase of gait. For anatomical factors, only EpA orientation and the origin of the collaterals were considered. Numerous studies investigating an

overall knee size concluded that the femoral width could be used to define a knee size [11, 17]. Therefore, EpW was used as a representative anatomical factor for the entire bone.

There were a few limitations associated with the study. Previous research has shown the effects of intra-prober variation in identifying anatomical landmark on the kinematics [74]. This could also affect the identification of anatomical factors used in this model. Cruciate ligaments play an important role in stabilizing the knee during both passive and active knee motions. Besides restricting tibial anterior-posterior motion, they also act as secondary stabilizers to the tibial I-E degree-of-freedom. The origin locations of both cruciates were difficult to identify and thus were not included in the PCA model. Another limitation of the study was that the insertion locations of none of the ligaments were included. Both medial and lateral collateral ligaments have long insertion sites and representing them in one point could have compromised the model accuracy. Despite these limitations, meaningful results were observed.

To highlight the usefulness of the coupled experimental and PCA approach, this study demonstrated that the V-V and I-E PCA models can help understand the relationship between envelope, gait kinematics and a few anatomical features. Approximately, half of the variation in the dataset was due to the relative position of the envelope, gait, EpA and collateral origin. Frontal plane angle of EpA and S-I location of LCL origin was associated with the envelop and gait shift. Whereas, transverse plane angle of EpA and A-P location of LCL origin was coupled with the I-E envelope and gait kinematics. One fourth of the variation was due to the size of the envelope, gait and EpW. Epicondylar width influenced the envelope size and the range of motion during gait. The model further predicted entire envelope and gait kinematics accurately and precisely using envelope boundaries at 10°, 50° and 100° and anatomical variables. It is

anticipated that results obtained here have potential benefits to implant designer and surgeons while making intra-surgery decisions about the implant alignment and ligament balancing.

4.5 Figures

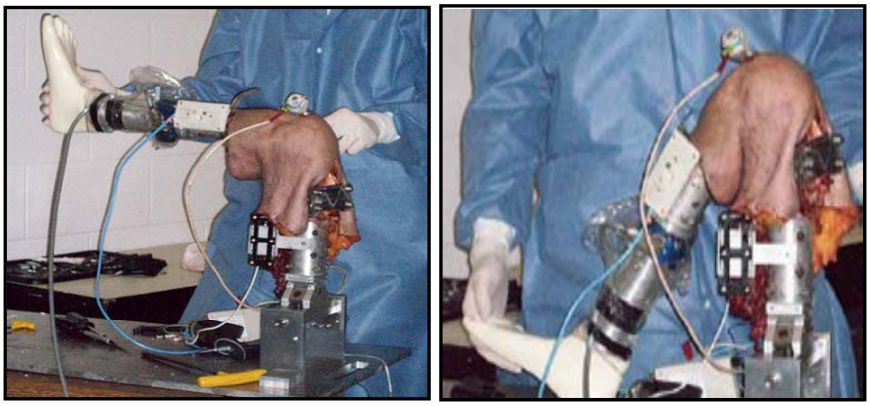

Figure 4.1: Experimental setup for tibial passive envelope of motion. Femur was fixed and tibia was free to move; moments were applied to the tibia while tibia was flexed from full extension to the terminal flexion. Tibiofemoral kinematics was captured using rigid bodies, which were mounted on the femoral and tibial fixtures.

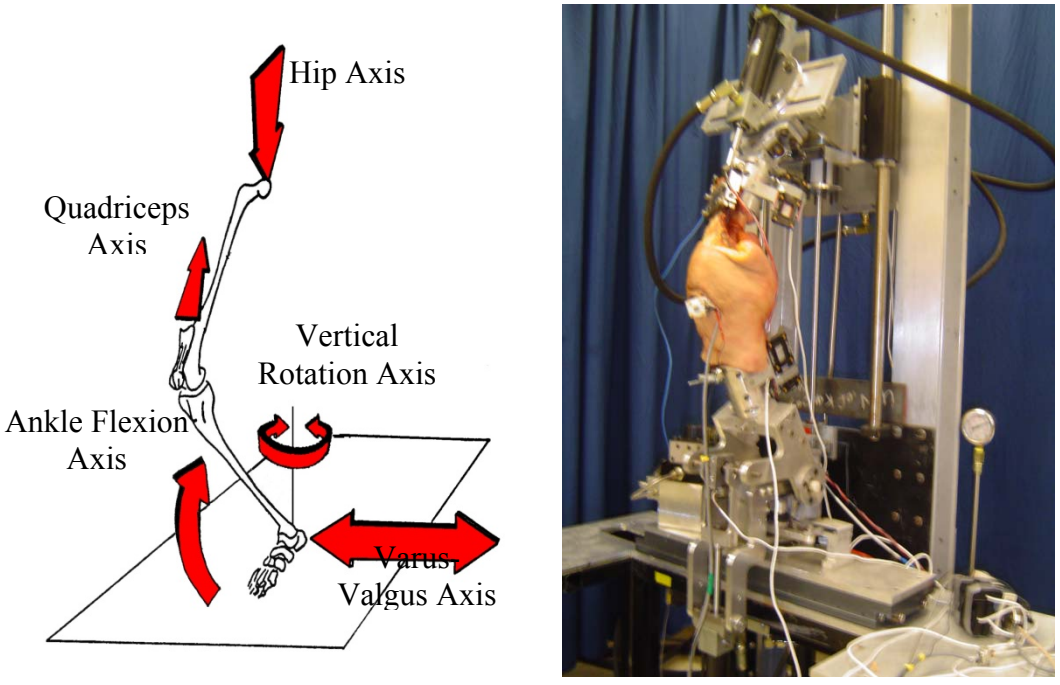

Figure 4.2: Forces applied to a knee in the Kansas Knee Simulator (left) and a cadaveric knee aligned in the KKS (right).

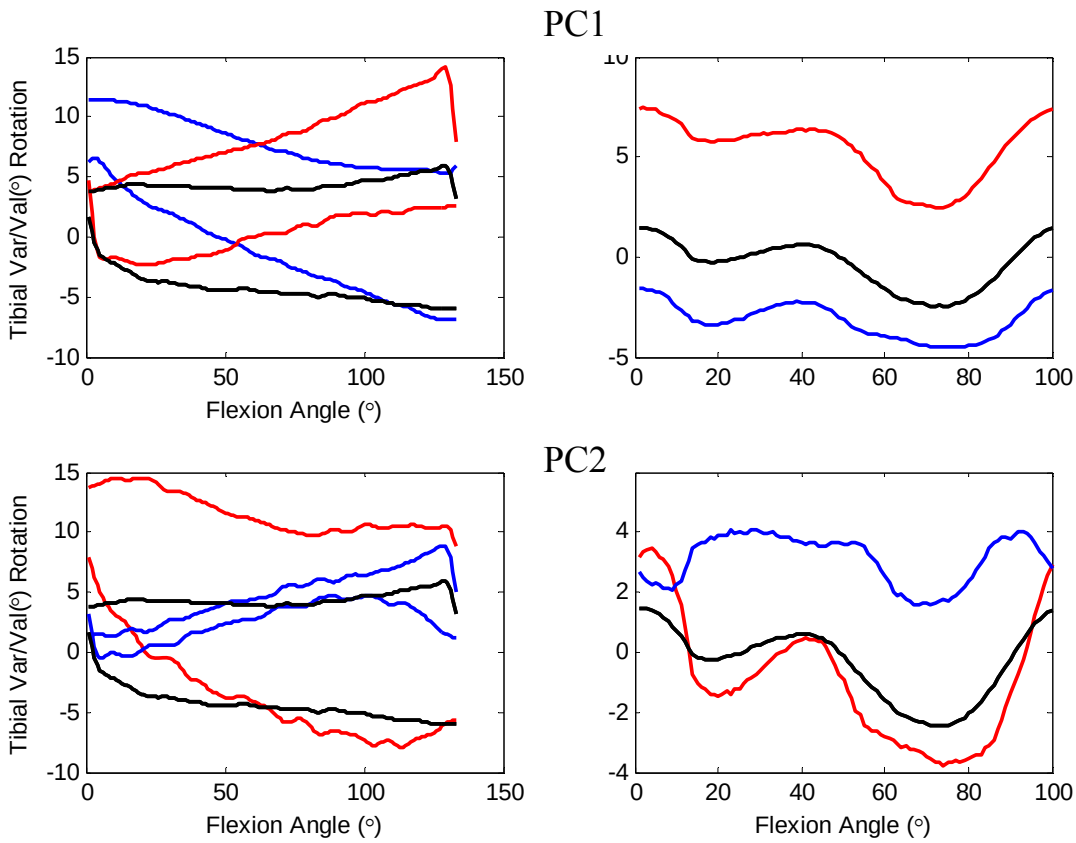

Figure 4.3: +3σ (red), mean (black) and -3σ (blue) deformation along the PC1 and PC2 axes for the V-V envelope (left) and gait (right). PC1 explained the variation in the dataset due to the relative position of the envelope and gait, whereas PC2 explained the envelope and gait size.

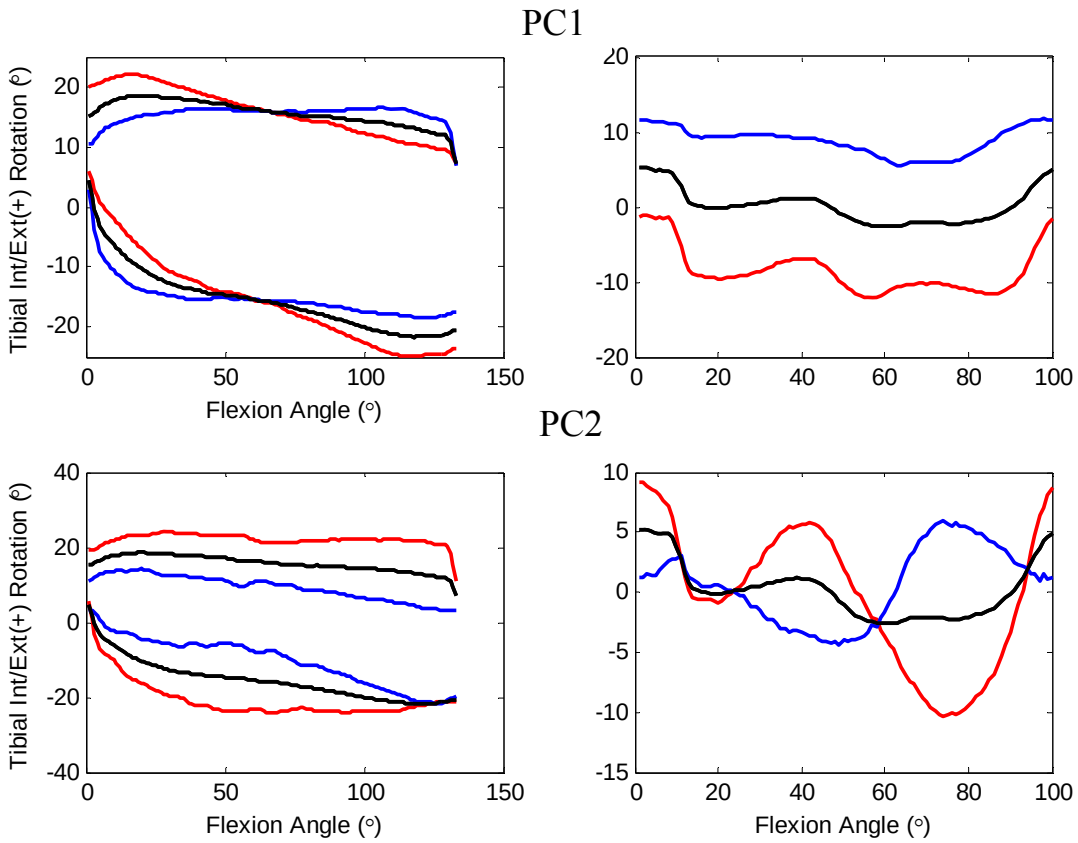

Figure 4.4: +3σ (red), mean (black) and -3σ (blue) deformation along the PC1 and PC2 axes for the I-E envelope (left) and gait (right). PC1 explained the variation in the dataset due to the relative position of the envelope and gait, whereas PC2 explained the envelope and gait size.

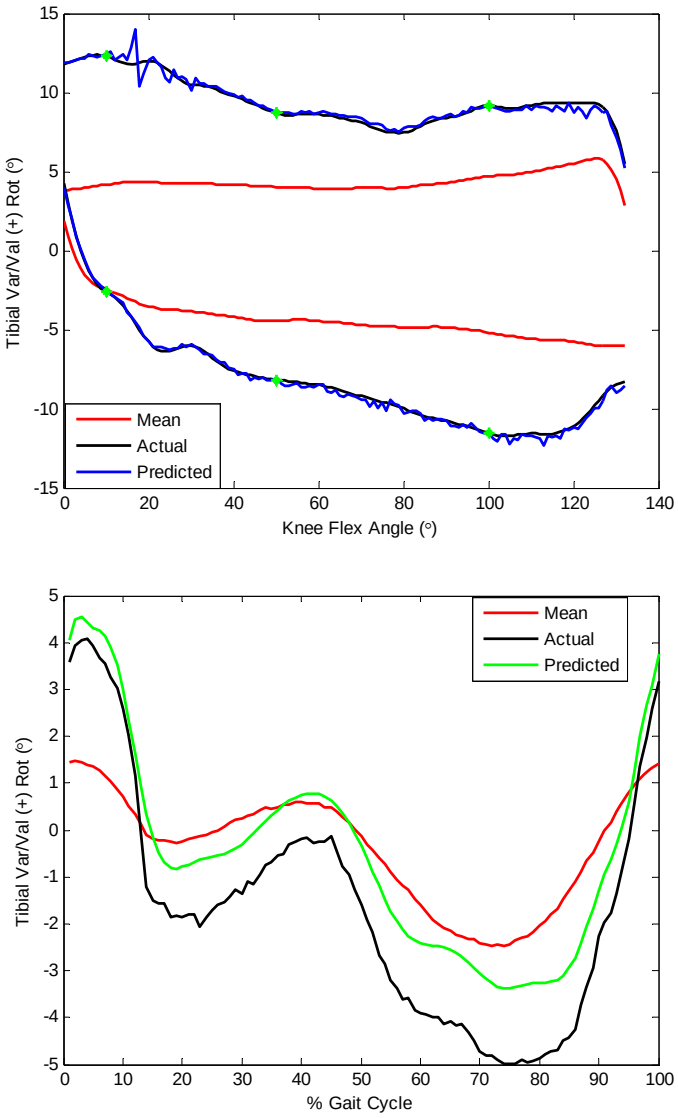

Figure 4.5: Mean (red), experimentally collected (black) and predicted (green) V-V motion of a random knee during envelope (top) and gait (bottom). Predictions were performed using a PCA based morphing algorithm. All anatomical measures and the envelope boundaries at 10°, 50° and 100° (green asterisk) were used for the envelope and gait prediction. No gait measures were included in the prediction. Mean RMS error for the envelope prediction was 0.5° and for the gait prediction was 1.2°.

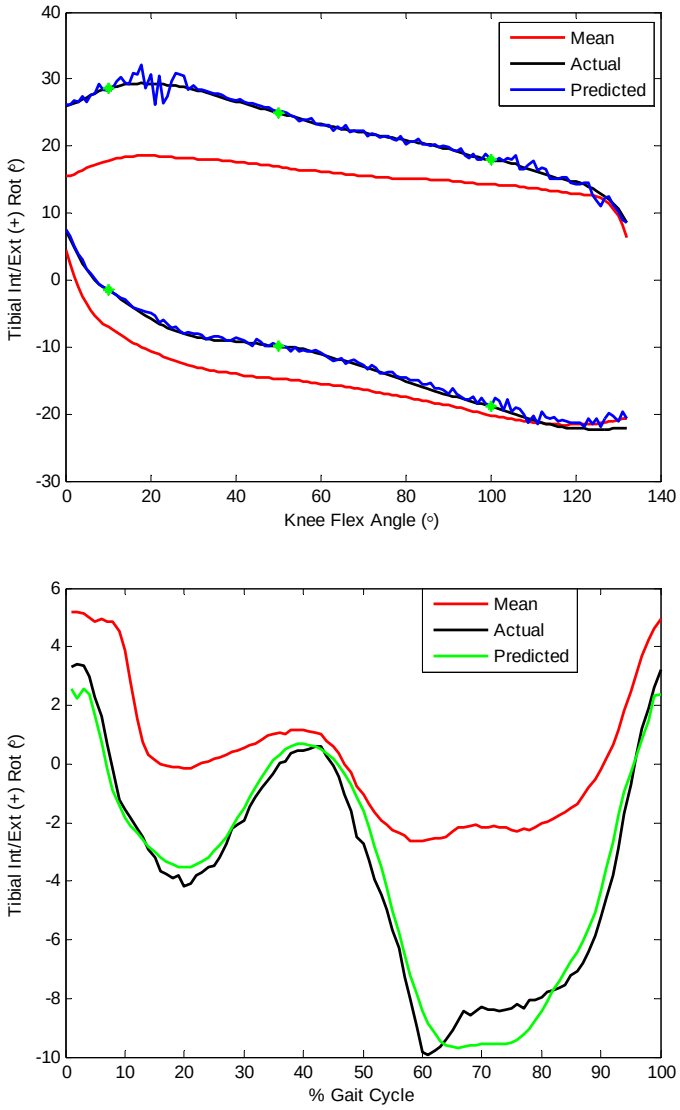

Figure 4.6: Mean (red), experimentally collected (black) and predicted (green) I-E motion of a random knee during envelope (top) and gait (bottom). Predictions were performed using a PCA based morphing algorithm. All anatomical measures and the envelope boundaries at 10°, 50° and 100° (green asterisk) were used for the envelope and gait prediction. No gait measures were included in the prediction. Mean RMS error for the envelope prediction was 0.7° and for the gait prediction was 0.8°.

4.6 Tables

Table 4.1: Percentage variation in the anatomy and envelope data explained by first three PCs along with their interpretation. Two separate models were developed for V-V and I-E motions. Three PCs explained about 90% of the variation in the dataset. FPA and TPA: Frontal and Transverse plane angle of epicondylar axis

	Principal components			Variation Interpretation		
	PC	**Variance**	**Cumulative**	**Envelope**	**Gait**	**Anatomical Factor**
V-V	PC1	49.0	49.0	shift	shift of a motion	FPA, S-I location of lateral EpA, S-I location of LCL
	PC2	35.2	84.2	Size	Magnitude of V-V range of motions	EpW, M-L location of both MCL and LCL
	PC3	7.8	92.0	Size and relative position	Magnitude of range of motion during stance phase	EpW and TPA, A-P location of MCL
I-E	PC1	51.8	51.8	shift	I-E shift of a motion	TPA, A-P location of lateral EpA, A-P location of both MCL and LCL
	PC2	24.7	76.5	Size	Magnitude of I-E range of motion	EpW, M-L location of both MCL and LCL
	PC3	14.8	91.3	Size and relative position	Magnitude of range of motion during stance phase	EpW and A-P location of both MCL and LCL

Table 4.2: Mean RMS error (°) for the envelope and gait predictions of V-V and I-E motions. For each knee, envelope and gait kinematics was predicted and later compared with the actual kinematics.

Knee	VV		IE	
	Envelope	Gait	Envelope	Gait
1	0.58	1.27	0.75	1.23
2	0.52	1.19	1.20	1.56
3	0.89	1.17	1.65	1.01
4	0.93	1.01	1.30	1.22
5	0.89	1.35	2.45	1.04
6	0.72	1.12	1.06	1.49
7	0.41	0.96	1.62	1.06
8	0.52	1.20	0.71	0.81
9	0.75	1.12	2.07	2.11
10	0.94	1.18	1.50	0.81
11	1.01	1.16	0.72	0.70
12	0.62	0.59	0.22	1.06
13	0.63	1.21	1.08	0.75
14	0.65	0.82	0.32	0.26
15	0.47	0.96	1.71	0.61
16	0.83	0.75	1.06	1.38
17	2.42	2.44	2.16	3.65

Appendix A:

The algorithm was developed and explained by the Styner *et al*. For PCA the mean model is the most probable surface. Therefore, the 'most probable surface' which satisfies the boundary conditions would be the surface which has minimal deviation from the mean. This objective function can be satisfied by minimizing the Mahalanobis-distance D_m.

To determine the most probable surface given the position of an arbitrary point *j*, the minimally Mahalanobis-distant surface $\vec{b}$ that contains the point *j* at the required position p_j must be found. So for all possible displacements p_j, a shape vector ϵ span(U) which translates the point *j* in direction (in the object space) would be seek, thereby only inducing a minimal deformation of the overall surface. More precisely, the shape vector shall be effect a unit displacement of the vertex *j* in the direction of a data point, and, as there are probably many such vectors, they shall be of minimal Mahalanobis-length D_m. Once the vector is found, one can satisfy all possible boundary conditions p_j with minimal deformation of the surface by just adding the appropriately weighted “basis" vector to the mean. This problem gives rise to the following constrained optimization:

Let $\boldsymbol{r}_j$ denote the unknown basis vector causing unit translation of point *j*. The mahalanobis-length D_m of this vector then given by:

$$D_m(\boldsymbol{r_k}) = (U_{r_k})^T \sum^{-1} U_{r_k} = r_k^T \wedge^{-1} r_k = \sum_{e=1}^{N-1} \frac{(r_k^{[e]})^2}{\lambda_e},\ k \epsilon \{x_j\}$$

Where, $\sum$ = covariance matrix

U = Eigenvectors

$\wedge$ = Diagonal matrix of eigenvalues

λ = Eigenvalue

Taking into account that x_j depend only on a row of U, Sub-matrix U_j is obtained from the following equation:

$$[xj] = \left[\overline{xj}\right] + \left[U^j\right] b = \left[\overline{xj}\right] + U^j b$$

Where, $U^j = J^{th}$ row of matrix U.

$b = U^T * P$ ... P = *Data matrix.*

To minimize the mahalonobis-distance D_m subject to the constraint of a decoupled translation by one unit, Lagrange function was introduced. This constrained optimization routine was solved using a Lagrange function (L_j) by Styner *et al*.

If the basis vectors and the Lagrange multiplier is combined according to $R_j = [r_j]$,

$$2 \wedge^{-1} R_j = U_j^T L_j \ldots\ldots\ldots\ldots (1)$$

$$U_j R_j = I \ldots\ldots\ldots\ldots (2)$$

If r_j is the basis vector, then result from simple algebraic operations (resolve (1) for R_j and replace R_j in (2) by the result), use the resulting equation to find $L_j = 2\left[U_j \wedge U_j^T\right]^{-1}$. Substitute for L_j in (1) and R_j is given by:

$$R_j = [r_{x_j}] = \wedge U_j^T \left[U_j \wedge U_j^T\right]^{-1}$$

While, r_j , describes the translation of x_j by one unit. The most probable surface $\tilde{p}$ given the displacement $[\Delta x]$ of an arbitrary data point j is then determined by,

$$\tilde{p} = \overline{p} + UR_j[x_j]$$

Before the next control point is considered, one must ensure that the subsequent modifications will not alter the previously obtained data and thus the components from the statistic that caused a displacement from previous point were removed. The variation coded by the point was subtracted from each instance *i*, and rebuild the statistic afterwards. For the first part of this operation, the basis vectors R_j weighted by the specific displacement $[\Delta x_j]^T_i$ was subtracted from each object instance

$$\tilde{b_i^j} = b_i - R_j\left[\Delta x_j\right] = b_i - R_j U_j b_i = (I - R_j U_j) b_i$$

Where, $b_i = U^T \Delta p_i$ and $\Delta p_i = p_i - \overline{p}$

After this step, a new data description that is invariant with respect to point *j* is obtained. In order to rebuild the statistic, a PCA to the normalized data $\{\tilde{b_i^j} \mid i \in \{1,...,N\}\}$ was applied. The point-normalized principal components, denoted by U^j, confirm the expected behavior and validate the removal of the variation in respect of point *j*.

The final most probable surface $\tilde{p}_l$ is given by reversing the point elimination procedure, that is, by combining the data information that is coded by the various control points. Accordingly, the mean surface $\overline{p}$ with all the weighted principal basis functions $R_{j_k}^{\tilde{s}_{k-1}}$ was combined

$$\tilde{p}_l = \overline{p} + \sum_{k=1}^{l} U^{\tilde{s}_{k-1}} R_{j_k}^{\tilde{s}_{k-1}} \left[\Delta x_{j_k}\right]$$

Therefore, final recursive data, $\tilde{p}_k$, will be obtained by,

$$\tilde{p}_k = \overline{p}_{k-1} + U^{\tilde{S}_{k-1}} R_{j_k}^{\tilde{s}_{k-1}} \left[\Delta x_{j_k}\right]$$

Chapter 5: Effect of Variability in Knee Anatomy and Implant Orientation on Knee Passive Envelope and Dynamically Simulated Gait: A Predictive Tool using Principal Components

5.1 Introduction

Total knee arthoplasty (TKA) is a highly successful procedure and generally considered to alleviate pain and restore functional kinematics [21, 75-77]. Numerous follow-up studies have demonstrated the high success rate and patient satisfaction of a TKA [76, 77]. The success of TKA could be influenced by numerous factors, including surgical techniques and the implant orientation during surgery. Significant variability associated with the femoral and tibial component rotational alignment has been reported in the literature [36, 78, 79]. Siston *et al.* found femoral rotational alignment ranging from 13.8º internal rotation to 16.8º external rotation [36], whereas, the tibial component rotational alignment in the transverse plane ranged from 44.8º internal rotation to 46.8º external rotation [80]. Numerous researchers have studied the effect of implant misalignment on knee kinematics and contact forces using both cadaveric and computational studies [36, 39, 78]. These studies, however, have typically altered a single parameter, thus interactions between alignment and kinematics variables were not considered. Furthermore, the combine effect of variability in the anatomy and implant orientation on the knee envelope and functional kinematics has not been studied.

The passive motion characteristics of the human knee-joint depend on the mechanical and structural interaction between the articular surfaces, the ligaments and other soft tissue structures [2, 3]. Because of its importance, the passive knee envelope is almost universally used as an intra and post-surgery stability assessment tool [3, 76]; however, the intra-surgery knee assessment could also be influenced by the implant orientation. During dynamic activities like walk and squat, a critical interaction occurs between dynamic muscle forces, compressive forces at the

joint and forces in the passive soft tissue to provide dynamic stability to the knee joint. It is believed that the active motions like walking and squatting are influenced by the passive envelop, it is also thought that the passive motion characteristics of a knee could assist in understanding the knee joint kinematics [2, 3]. Researchers have attempted to determine the interaction between the passive envelope and active kinematics of a native knee, though with limited success due to inter-subject variability, the loading-rig dependant methodology and computational model's sensitivity to the input variables [47]. Furthermore, since the post-TKA knee joint kinematics during both the envelope assessment and functional activity are believed to be influenced by the implant orientation, its effect on the outcome kinematics must be studied.

Principal component analysis (PCA) is a statistical tool that has become quite popular in the analysis of multivariate data. The aim of a PCA is to reduce the dimensionality of a multivariate data set while retaining as much variation as possible. Several authors have demonstrated the usefulness of PCA in knee biomechanics to reduce the dimensionality and explain inter-subject variability of the gait waveform [11, 49, 66]. Moreover, the technique has been widely accepted in shape morphing algorithms; the modeling method used to obtain a complete surface model from sparse data points [55, 81]. Styner *et al.* further modified a PCA based morphing technique by operating directly in the PCA shape space incorporating large sets of possible variations including parameters additionally to the spatial and non-spatial information such as patient height, weight, age, etc. [82].

A statistical tool can be used to understand the relationship between various factors in the implant orientation, knee anatomical features, its envelope and joint kinematics during weight-bearing activities. Moreover, once the model is generated, a morphing scheme can be used to predict the tibiofemoral kinematics during various activities using a small subset of the implant

orientation, anatomical measures and the envelope measures. In the prediction algorithm, like shape prediction, tibiofemoral kinematics will be considered as a shape to be predicted, whereas the implant orientation, anatomical and envelope measures will be treated as a sparse data points. The primary objective of this research was to examine the correlation between the variation in the knee anatomical factors and the implant orientation factors with observed tibiofemoral kinematics during a passive knee envelope and simulated dynamic activities. The second objective was to identify the orientation, anatomical and envelope factors that explain the maximum variation in the tibiofemoral kinematics during gait and use them to predict knee kinematics using PCA based morphing algorithm.

5.2 Materials and Methods

5.2.1 Experimental Setup

Ten fresh frozen cadaver legs (age: 63.3±9.9, BMI: 29.1±4.3) were thawed at room temperature and then dissected. For each leg, the femur and tibia were sectioned 28 cm proximal and 18 cm distal to the epicondylar axis. All soft tissue within 10 cm of the knee joint was left intact to prevent the dehydration of the tissue. Soft tissue more than 10 cm from the epicondylar axis was removed, with the exception of the multiple heads of the quadriceps tendons. Remainders of the tibia and femur were cleaned and cemented into tubular fixtures aligned parallel to the bones' intermedulary canals. All knees were later implanted with the Posterior Stabilized (PS) design (∑ PS Fixed, DePuy Inc.) by the Orthopaedic board approved surgeons.

For the passive envelope of motion, the femur was fixed leaving the tibia to move freely (Fig. 5.1). An assessment was performed manually by moving the tibia though the flexion-extension (F-E) range of motion (ROM) from full extension to full flexion. During the F-E ROM, loads and torques were applied until the tibial varus-valgus (V-V) and internal-external (I-E) motion

was constrained. The constraint was felt by the researcher's tactile sensations and may not be a clear end point of that motion. Care was taken while applying the loads in order to avoid damaging the soft tissue around the joint. After the envelope assessment, the knee underwent a dynamically simulated gait cycle in the Kansas Knee Simulator (KKS) (Fig. 5.2) [69]. The Kansas Knee Simulator has five axes of control: 1) a vertical load at the hip, 2) a quadriceps load, 3) a torque about a vertical axis through the ankle, 4) a medial-lateral ankle force, and 5) an ankle flexion moment. The knees underwent simulated walking using 50% bodyweight derived from an ISO standard [83]. Knees were aligned in the KKS during squatting to maintain a vertical orientation of the tibia and minimize tibial I-E rotation and mediolateral (M-L) translation of the ankle. The alignment adjustments included V-V angle and I-E rotation of the femur relative to the hip and I-E rotation of the tibia relative to the ankle. The quadriceps actuator could translate and rotate in the frontal plane and was aligned with long axis of the femur and the center of the patella.

Tibiofemoral motions were captured during the assessments by tracking rigid arrays of infrared-light emitting diodes mounted to the tibial and femoral fixtures using an Optotrak 3020 camera system (NDI, Waterloo, Canada). Reported accuracy of the system is 0.5mm and 0.5º [58]. Several anatomical landmarks were identified and their locations were captured using a digital stylus. Tibiofemoral kinematics were described using Grood and Suntay knee kinematics description [59].

5.2.2 Obtaining Anatomical and Implant Orientation Variables

After testing, the knees were dissected down to the joint capsule and attachment locations of the medial and lateral collateral ligaments and medial and lateral epicondylar axis were recorded using a digital stylus. Series of points were collected at the collateral's origin sites and the

centroid of these points was used for the analysis. Also, locations of the medial and lateral epicondylar axis (EpA) were identified with the manual assessment and recorded. Later, the Cartesian coordinates of these points were described in the femoral coordinate frame. Using medial and lateral epicondylar points the epicondylar width (EpW), its frontal plane angle (FPA) and transverse plane angle (TPA) with respect to the femoral coordinate frames were estimated.

For implant orientation, distinct geometrical features along with the point cloud were collected on the femoral and tibial implant articulating surfaces. The Cartesian coordinates of the implant corner points were used to define consistent femoral and tibial implant coordinate frames across the knees. Later, angular orientations of the implant coordinate frames were obtained in the Grood and Suntay anatomical coordinate frame of the respective bone. The femoral implant's orientation included its F-E, V-V and I-E rotation, whereas, tibial orientation summarized its posterior slope (F-E), V-V slope and I-E rotation.

5.2.3 PCA Model Development

One aim of a PCA is to reduce the dimensionality of a multivariate dataset while retaining as much variation as possible. PCA defines a linear transformation that decorrelates the parameter signals of the original data by projecting the objects into a linear data space spanned by a complete set of orthogonal basis vectors (PCs). If the variables are highly correlated, then the major variations in the dataset are described by the first few basic vectors. In this study, a PCA model would separate and quantify the major variation in the data that occurs within the population of the cadaver's envelope and gait kinematic data.

Two separate PC models were developed for the V-V and I-E rotations. Achieved envelope boundaries were identified at each 1º of knee flexion angle and kinematics at each 1% of the gait cycle. The data matrix consisted of $\boldsymbol{N}$ cadavers ($\boldsymbol{N}$=10), with $\boldsymbol{n}$ variables defining anatomical,

implant orientation, envelope and gait kinematics variables. Cartesian coordinates of the medial and lateral epicondylar points, and origins of medial and lateral collateral ligaments along with EpW, FPA and TPA described the anatomical variables (n_1=15). Angular orientations of each implant relative to its respective bone coordinate frame summarized implant orientation variables (n_2=6). Envelope variables were maximum and minimum point of the envelope at each 1º of flexion angle (0º-120º, n_3=242), whereas, gait variables were tibiofemoral kinematics at each 1% of gait cycle (n_4=101). Hence each cadaver x_i (i = 1, 2, …, N) was represented by n (n= $358, n_1+ n_{2+} n_{3+} n_4$) data variables. Let P be the $N \times n$ matrix, each column holding the variables for one subject. Since the input matrix contains variables with different units, a *z*-score matrix was calculated, which was used for subsequent calculations. Once PCA was performed, *z matrix* was transformed back into the original basis of all the input variables. A $n \times n$ covariance matrix C was constructed with entry $C_{a,b}$ containing the covariance between row a and row b of matrix P. The eigenvectors and corresponding eigenvalues of matrix C were . Each column of matrix E, the eigenvector matrix, held an eigenvector e_l (l = 1, 2, …, n) of matrix C. The eigenvectors of C were the PCs of the data. The mean of each variable was calculated and stored in $1 \times n$ row vector V_{mean}. The PC scores were calculated as the dot product of the PC and the variables. Let P_{mean} be $1 \times n$ column vector containing the PC scores of the mean variables. Thus,

$$V_{mean} . E = P_{mean} \quad \text{(Eq 1)}$$

The PC scores P_{mean} can be altered and the corresponding deformation V of the input kinematic and geometric variables can be calculated and displayed according to:

$$V = P . E^{-1} \quad \text{(Eq 2)}$$

Where, $E. E^{-1} = I_n$, the identity matrix.

The range through which the PC scores could be altered was limited to ± three standard deviations so that the effects of envelope boundaries on the envelope can be visualized.

PC model results included the PCs and the variance explained by them. The model was further deformed (within ±3σ) along each PC axis with all other PCs fixed at the mean, to identify the variation associated with that specific PC. Envelope changes associated with the PC would be coupled with the corresponding changes in the anatomical and implant orientation factors along with the envelope and gait kinematics. If anatomical and implant orientation factor changed more than ±50% from its mean value, it was considered to be the factor coupled to the corresponding change in the envelope and gait kinematics. The PC interpretation process was continued until 95% of the variation in the input data matrix was explained. One should remember that the variation associated with each PC is an interpretation of that PC; the trends observed in the dataset without their quantification.

5.2.4 Kinematics prediction from envelope measures using PCA model

Styner *et al.* developed a novel bone morphing scheme operating directly in the PCA shape space and incorporating a large set of possible variations in parameters in addition to specific information such as patient height, weight, age etc. [82]. The method is based on the iterative removal of shape information associated with the digitized points. First, the most probable shape subject to the boundary conditions that are related to the initially digitized landmark was calculated. The resulting outline was used for registration and as an initial configuration for computing the most probable shape for the next digitized point. Using statistical shape analysis, the remaining shape variability was examined, after the surface information coded by the digitized points is progressively subtracted. This procedure of point selection and variability removal was repeated until a close approximation to the patient anatomy was achieved. The final

extrapolated surface represented the most probable surface in the shape space given the digitized landmarks. The mathematical algorithm is described in Appendix A.

The proposed prediction model operates in the eigenvector space and can handle both spatial and non-spatial datasets. Predictions were performed using all anatomical variables and minimum and maximum boundaries of the envelope at 10°, 50° and 100° of knee flexion. Selected anatomical, implant orientation and envelope measures, considered as shape landmarks, were used to obtain entire envelope and gait kinematics, considered as a complete shape, by calculating most probable shape subjected to the boundary condition described by the implant orientation, anatomical and envelope measures.

The leave-one-out analysis was carried out to evaluate the accuracy and reproducibility of the prediction algorithm. For I-E and V-V kinematics, entire envelope and tibiofemoral kinematics during gait were predicted using implant and anatomical features and the envelope boundaries at 10°, 50° and 100° of knee flexion. Each of these angles were considered as a representative flexion angle during stance and swing phases of the gait. The RMS error between predicted and experimentally collected envelope and kinematics was calculated for each prediction. A small magnitude of the RMS error would ensure the accuracy and precision of the morphing algorithm.

5.3 Results

Results of V-V and I-E PC model with anatomical and implant orientation features along with the envelope and gait kinematics are summarized in Table 5.1.

5.3.1 V-V PCA Model

Four PCs explained 95.5% of the variation in the V-V dataset (Table 5.1). PC1 captured variation in the relative position of the envelope and gait, explaining 50.9% of the variation (Fig. 5.3). Envelope and gait relative position also changed with the FPA and S-I location of EpA and

LCL origin. The variation was tied with the femoral component's I-E alignment. Deformation along the PC1 axis showed that the valgus shift in the envelope was coupled with the valgus shift in gait (Fig. 5.3). This valgus shift was observed with the superior location of LCL and EpA, which essentially increased the FPA. Tibial orientation did not change with the valgus orientation of the envelope and gait; however, reduction in the femoral external rotation was observed. Similarly, the varus shift of an envelope occurred with the varus shift of gait and inferior location of LCL and EpA with reduced FPA along with the femoral external rotation.

PC2 captured 24.2% variation summarizing varying size of the envelope and range of motion during gait. PC2 also explained the variation in the EpW and the M-L location of MCL and LCL origin (Table 5.1). Furthermore, the changes were tied with the tibial V-V slope. Deformation along PC2 axis demonstrated the increase in envelope size with its V-V alignment and the increase in the range of motion during gait (Fig. 5.3). Moreover, the change was tied with the increasing EpW and the M-L locations of both collaterals along with the valgus slope of the tibial implant. Although the variance explained by PC3 and PC4 was low, they summarized important relationships between the variables (Table 5.1). PC3 summarized the variation in the envelope size at mid-flexion and the range of motion during gait at swing phase, which was associated with the A-P location of the collateral origins and the F-E alignment of the femoral implant. PC4 explained only 9% of the variation in the dataset summarizing a varus shift of the envelope at early flexion and a varus shift during gait at stance phase, along with a reduced tibial external rotation.

5.3.2 I-E PCA Model

Four PCs explained 95.0% of the variation in the I-E dataset (Table 5.1). The first PC captured variation in the relative position of the envelope and gait, explaining 50.6% of the

variation (Fig. 5.4). The change was coupled with the varying TPA and A-P location of EpA and both collaterals with the I-E alignment of the tibial implant. When the PC1 was deformed between ±3σ, an externally shifted envelope was observed with the externally shifted gait waveform (Fig. 5.4). The change was coupled with the increasing external alignment of the tibial implant and increasing TPA, due to the posterior shift of the lateral EpA and LCL origin with the anterior shift of the MCL origin. None of the femoral rotational alignments showed to influence the observed variation in the I-E envelope and gait kinematics.

PC2 captured 34.7% variation in the dataset and was due to the varying sizes of the envelope and the range of motion during gait with its temporal shift of peak internal rotation. The variation was observed with the EpW and the M-L locations of both collaterals along with the femoral implant I-E rotational alignment. Deformation along the PC2 axis showed that the increase in EpW occurred with the femoral external rotation and increase in the envelope size and I-E range of motion during gait. PC3 and PC4 captured 6% and 4% of the variation respectively. PC3 explained the relationship between envelope size at mid-flexion and range of motion during gait at swing phase, which occurred with the femoral implant's F-E alignment. Whereas, PC4 summarized the internal shift of the envelope at early flexion and the internal shift during gait at stance phase, along with the reduced tibial varus slope.

5.3.3 Kinematics Prediction and Model Validation

Leave-one-out analysis was carried out to estimate and compare the predicted outcomes. The PCA model was built using nine samples to predict the envelope and kinematics of the left-out sample. The V-V (Fig. 5.5) and I-E (Fig. 5.6) envelope and gait kinematics was predicted using a few envelope measures (envelope boundaries at 10°, 50° and 90° flexion), anatomical features and implant orientation features. For the V-V model, the RMS error for the envelope and gait

kinematics was 0.4° and 0.2° respectively (Fig. 5.5). Whereas, for the I-E model, RMS error for the envelope and gait kinematics was 0.8° and 0.2° respectively (Fig. 5.6). In order to estimate the reproducibility of the prediction, leave-one-out analysis was performed and the envelope and gait kinematics of the left out knee was predicted. Predicted kinematics was compared with the experimentally collected kinematics and the mean RMS error for both V-V and I-E envelope and gait was estimated (Table 5.2).

5.4 Discussion

Despite the high reported variability in rotational alignment of the femoral and tibial components, its effect on tibiofemoral kinematics, both passive (envelope) and active (gait) is not clear in the literature. A few researchers studied the effect of tibial and femoral malrotation on the tibiofemoral contact forces using cadaveric and computational models [36, 39, 79]. These studies, however, have altered a single parameter, thus interactions between alignment and kinematics were not considered. Furthermore, the combine effects of malrotation on the passive envelope and kinematics during functional activities is not reported. The study summarized variation in the post-TKA tibiofemoral envelope, gait kinematics, anatomical variables and the implant orientation variables using principal component analysis. Moreover, a morphing algorithm was implemented to predict entire envelope and gait kinematics using a few envelope measures and all anatomical and implant orientation features.

For both V-V and I-E models, half of the variation was captured by the first PC and was due the relative position of the envelope and gait (Fig. 5.3 and Fig 5.4). Deformation along PC1 axis showed stronger relationship between the orientation of the tibial implant and the relative position of kinematics. For V-V motion, a valgus shift of the envelope and gait kinematics was observed with the reduced external rotation of femoral implant. Rotational alignment of the

femoral implant has been reported to affect the knee kinematics. In two different cadaveric studies, Miller *et al*. [84] and Anouchi *et al.* [39] observed that internally rotated femurs shifted the tibiofemoral kinematics more valgus, whereas, externally rotated femur shifted kinematics more varus. In his computational simulation model, Siston *et al.* [36] observed similar results and reported that the internally rotated femur not only shifted the functional activities more valgus, it also increased the MCL strain by small amount. However, the group also summarized that patients would alter their gait and uses the compensatory mechanisms, such as changing center of gravity and firing semimembranosus muscle group, to increase varus moment and reduce the MCL strain.

Deformation along the PC1 axis of an I-E model showed that the externally shifted envelope and gait was associated with the external orientation of the tibial implant. Numerous studies have been performed to understand the effect of tibial implant's I-E alignment on contact forces, contact stresses and post-TKA kinematics [24, 78, 79, 85]. Using a computational model Siston *et al.* found that the externally rotated tibia biases the position of femoral component, which could potentially constrain the tibial internal rotation or encourage tibial external rotation [33, 36, 86]. During surgery, surgeons usually follow different philosophies while determining the rotational alignment of the tibial implant. Misalignments can occur while determining this position, ranging from 44º internal rotation to the 46º external rotation [80]. Although the variation in the tibial I-E alignment observed in this study was not in these ranges, it was large enough to be captured by the first PC.

A few interesting trends between the anatomical factors and the envelope and gait kinematics were observed. The change in the relative position of envelope and gait was associated with the orientation of the EpA, FPA for V-V and TPA for I-E models. FPA changed with the change in

S-I location of the lateral EpA and LCL origin; whereas, change in TPA was coupled with the A-P location of medial and lateral EpA with both LCL and MCL origin. This indicates that the location of MCL and LCL origin changed in the direction of the orientation of EpA, which means the collateral origins are closely associated with the location of medial and lateral EpA and were contributing factors to the orientation of envelope and gait kinematics.

Second PC for both V-V and I-E models captured the variation in the envelope size and the range of motion during gait (Fig. 5.3 and Fig. 5.4). For V-V model, the size variation was coupled with the V-V slope of the tibial implant. PC axis deformation showed that the increase in the envelope size and gait range of motion was linked to the increase in the valgus slope of the tibial insert. Increase in tibial valgus slope opens the medial compartment more than the lateral, which could potentially reduce the strain on the soft tissues from the medial compartment. Reduced strain, which could lead to the lesser stiffness of the soft tissue, may have played a role in increased V-V envelope and gait kinematics. For I-E model, increase in the envelope and gait size was coupled with the femoral external rotation. While aligning the femoral implant, surgeons usually rotate the implant externally [87, 88]. Studies have shown that the external rotation of the femoral component decreases the lateral flexion gap without creating an abnormally increased medial flexion gap, which reduces possibility of straining collateral ligaments [39]. This indicates that the size of V-V and I-E envelope and gait was influenced by the component orientation factors which do not strain the soft tissue structures. Changing envelope and gait size was associated with the EpW and the M-L location of the collateral origins. Thus, it can be inferred that the increase in the EpW was associated with the larger envelopes which was related to the range of motion during gait.

For both V-V and I-E models, variance explained by the subsequent PCs was relatively small; however, they characterized a few interesting behaviors in the dataset. PC3 for both motions summarized the size of envelope at mid-flexion and gait at swing phase. Deformation of the PC axis showed that the femoral implant's flexion-extension alignment affected this mid-flexion change. Flexed implant position increased the size of both envelope and gait at mid-flexion. A flexed alignment of the femoral implant would alter the tibiofemoral articulation, which could have increased the envelope size at mid-flexion and at swing phase. PC4 summarized the varus and internal shift of the envelope at early flexion and was coupled with the tibial implant's I-E and V-V orientation respectively.

Several intra-surgery and post-surgery factors influences the post-TKA kinematics. The influence of anatomical factors, which remain unchanged pre and post-surgery, on the post-TKA kinematics is not reported in the literature. This study summarized how a few anatomical factors affected the kinematics; however, it was difficult to distinguish the effects of anatomical and implant orientation factors on the kinematics individually. During stance phase of a gait cycle, compressive load at a knee joint can reach up to three times bodyweight. Under such a high compressive load and quadriceps force, tibiofemoral stability is achieved by the dynamic knee stabilizer; however, ligaments and other soft tissue structures play an important role in restricting joint motion. The passive envelope of motion characterizes these soft tissue structures. During swing phase of gait, there is limited load across a knee joint and the tibiofemoral motion is a passive motion, which is partially driven by the passive knee structures. Therefore, in both stance and swing phase of gait, envelope factors plays an important role, which was quantified by the PCA model developed here.

The dataset used for this study included both spatial and non-spatial data; such as kinematics, implant orientation, Cartesian coordinates of the EpA and ligament origins (spatial) and EpW, FPA, TPA (non-spatial). A PCA based bone morphing algorithm used a few landmarks to predict the entire bone shape. Selective implant orientation, anatomical and envelope measures, considered as shape landmarks, were used to obtain entire envelope and gait kinematics, considered as a complete shape, by calculating most probable dataset subjected to the boundary condition described by the anatomical and envelope measures. The algorithm predicted entire envelope and a gait kinematics accurately and precisely (Fig. 5.5, Fig. 5.6 and Table 5.2).

For envelope measures, the achieved minimum and maximum envelope boundaries at 10°, 50° and 100° knee flexion were obtained. Each of these flexion angles are representative of the range of flexion angles during stance and swing phase of gait. For anatomical factors, only EpA and origin of collaterals were considered. Numerous studies investigating an overall knee size concluded that the femoral width could be used to define a knee size [89]. Also, stronger correlations between femoral width and cruciates size have been established [8]. Therefore, EpW was used as a representative anatomical factor for the entire bone. Since the insertion points of the cruciates and other soft tissues were difficult to identify accurately, they were not considered in the dataset.

There were few limitations associated with the study. Previous research has shown the effects of intra-prober variation in identifying anatomical landmark on the kinematics [74, 90, 91]. This could also affect the identification of anatomical and implant orientation factors used in this model. Another limitation of this study was the sample size. Ten cadavers were used to develop the PCA model, which could be considered as a small sample size for the included number of

variables. Another limitation of the study was that the insertion locations of both collateral ligaments were not included. Both medial and lateral collateral ligaments have long insertion sites and representing them in one point could have compromised the model accuracy. Despite these limitations, meaningful results were observed.

To highlight the usefulness of the coupled experimental and PCA approach, this study demonstrated that the V-V and I-E PCA models can help understand the relationship between envelope, gait kinematics, implant orientation and a few anatomical features. Approximately, half of the variation in the dataset was due to the relative position of the envelope, gait, EpA and collateral origin. Femoral component's I-E alignment, frontal plane angle of EpA and S-I location of LCL origin was associated with the orientation of both V-V envelop and gait kinematics. Whereas, tibial implant's I-E alignment, transverse plane angle of EpA and A-P location of LCL origin was coupled with the I-E envelope and gait kinematics. One fourth of the variation was due to the size of the envelope, gait and EpW. Tibial implant's V-V slope and femoral implant's I-E alignment was coupled with the size and V-V and I-E envelope respectively. Furthermore, the size of epicondylar width influenced the envelope size and the range of motion during gait. The model was further developed to predict entire envelope and gait kinematics accurately and precisely using envelope boundaries at 10°, 50° and 100° and anatomical variables. It is anticipated that results obtained here have potential benefits to surgeons while making intra-surgery decisions about the implant alignment and ligament balancing.

5.5 Figures

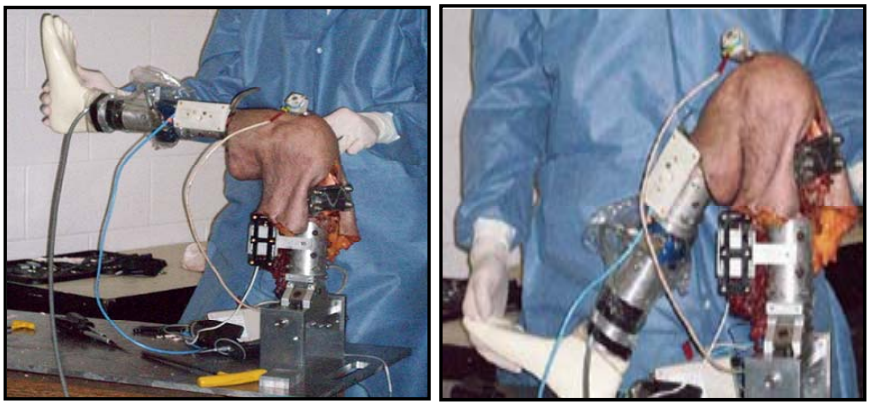

Figure 5.1: Experimental setup for tibial passive envelope of motion. Femur was fixed and tibia was free to move; moments were applied to the tibia while tibia was flexed from full extension to the terminal flexion. Tibiofemoral kinematics was captured using rigid bodies, which were mounted on the femoral and tibial fixtures.

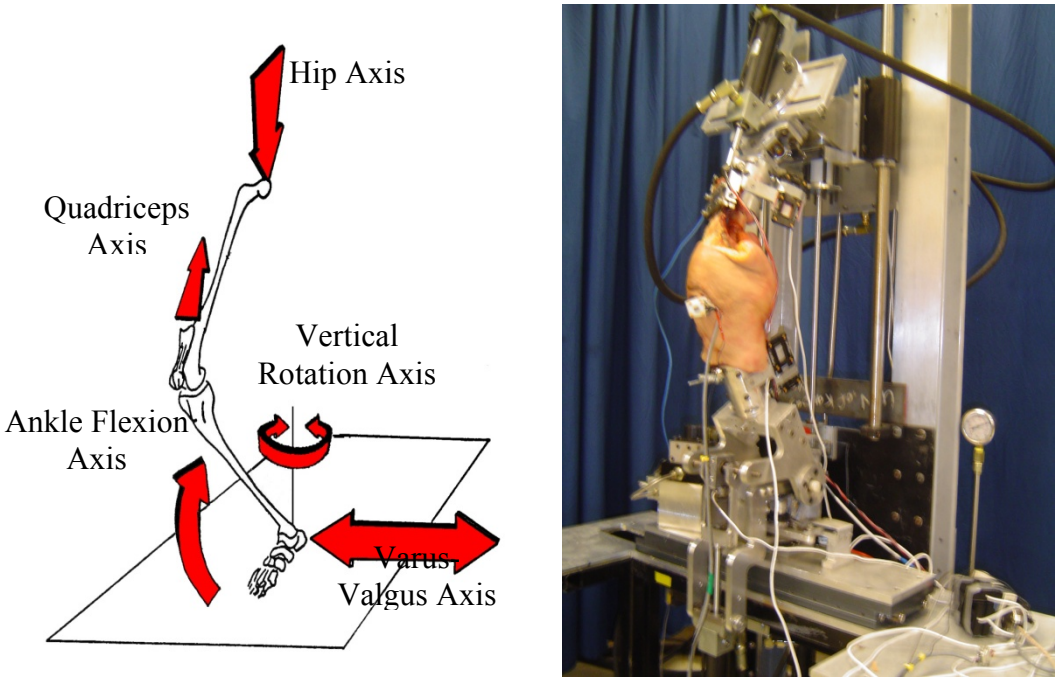

Figure 5.2: Forces applied to a knee in the Kansas knee simulator (left) and a cadaveric knee aligned in the KKS (right).

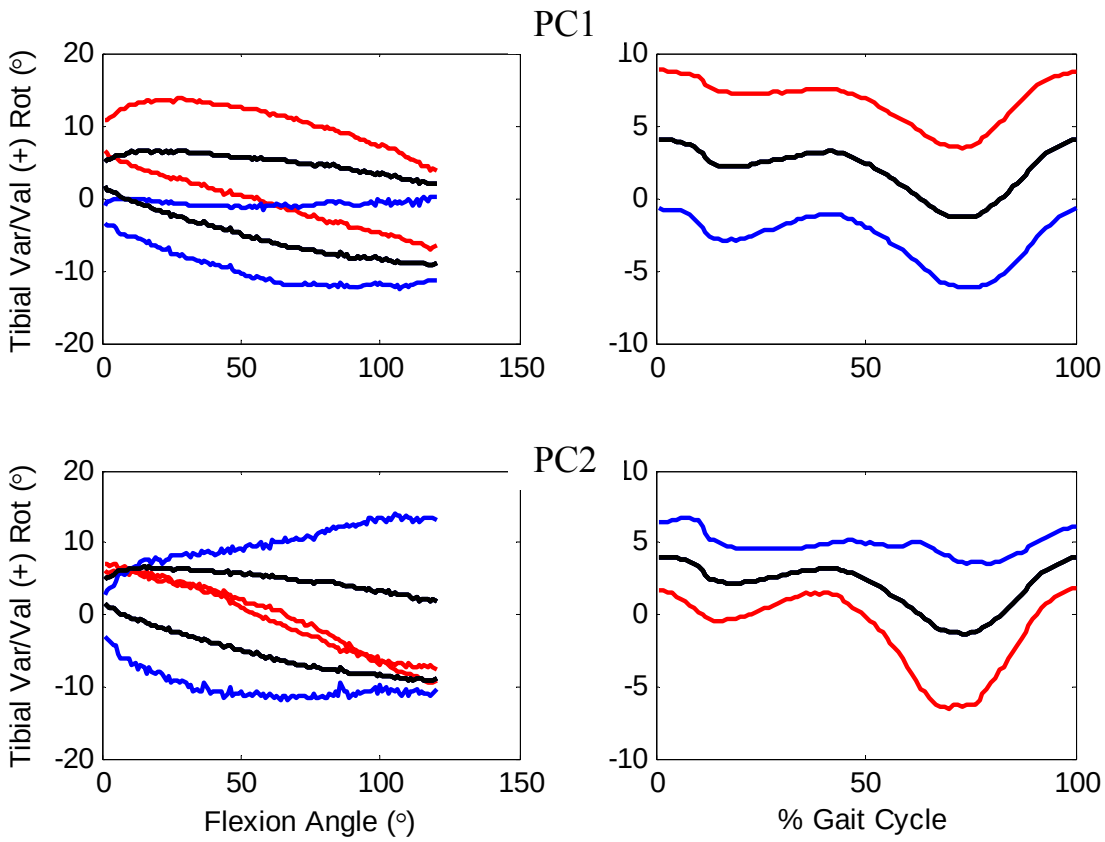

Figure 5.3: +3σ (blue), mean (black) and -3σ (red) deformation along the PC1 and PC2 axes for the V-V envelope (left) and gait (right). PC1 explained the variation in the dataset due to the relative position of the envelope and gait, whereas PC2 explained the envelope and gait size.

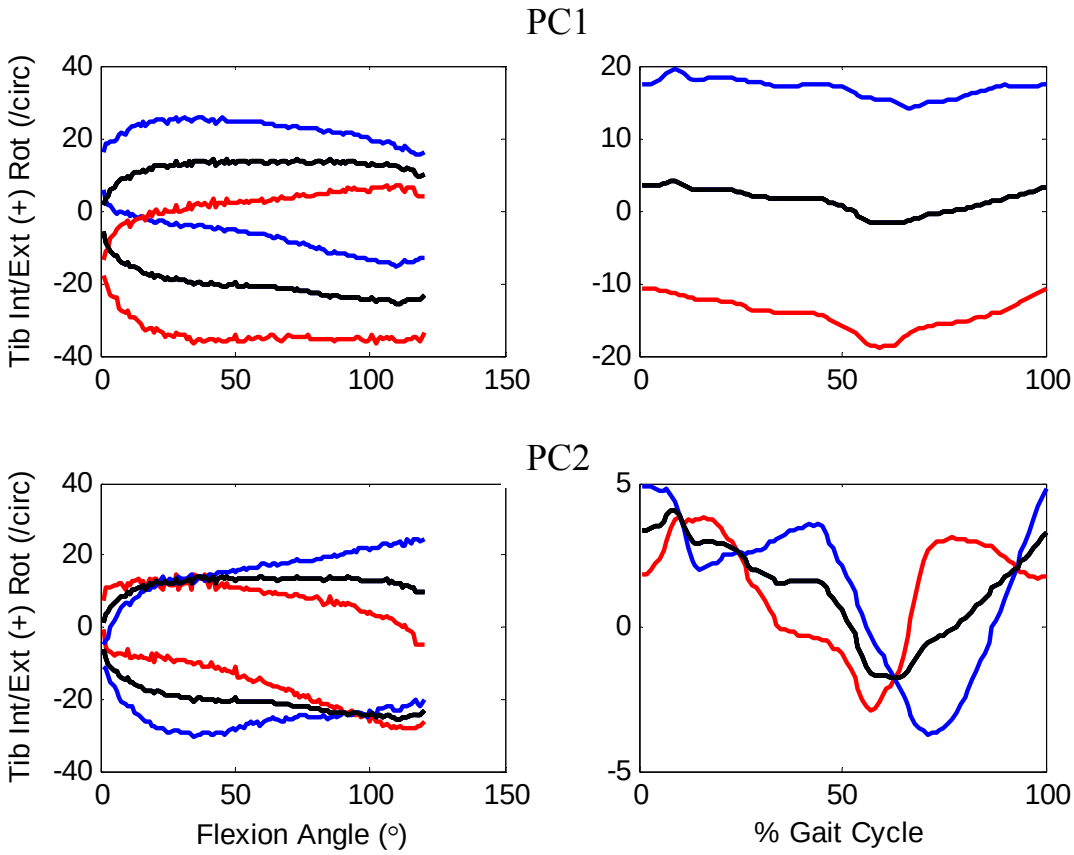

Figure 5.4: +3σ (blue), mean (black) and -3σ (red) deformation along the PC1 and PC2 axes for the I-E envelope (left) and gait (right). PC1 explained the variation in the dataset due to the relative position of the envelope and gait, whereas PC2 explained the envelope size and temporal shift in the peak tibial internal rotation during gait.

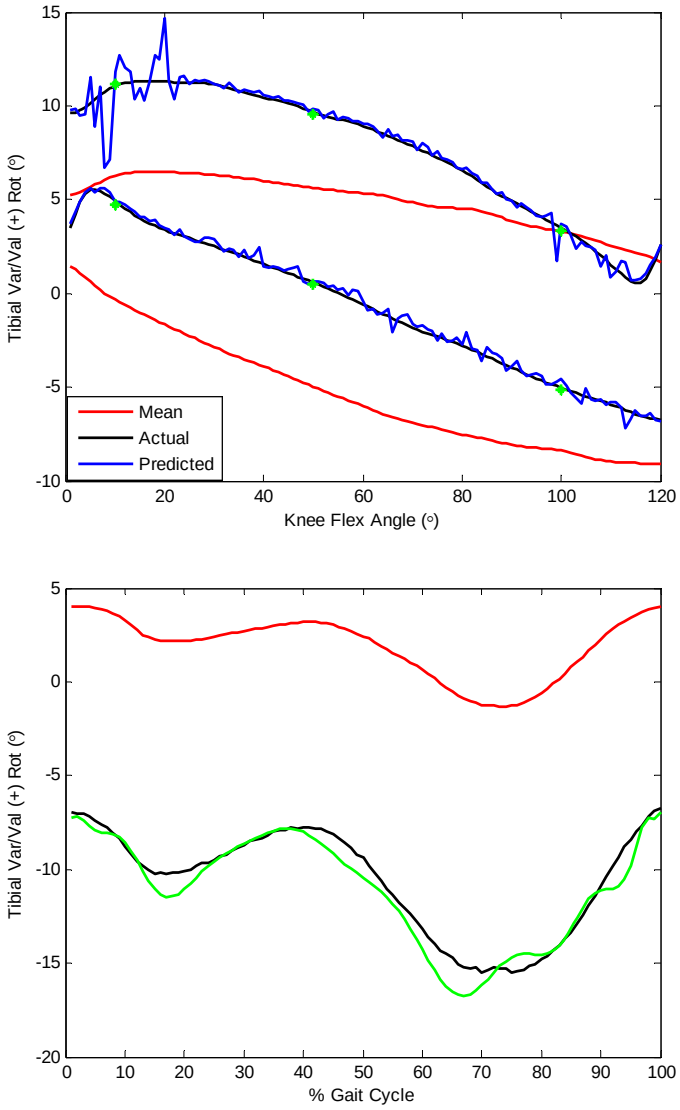

Figure 5.5: Mean (red), experimentally collected (black) and predicted (green) V-V motion of a random knee during envelope (top) and gait (bottom). Predictions were performed using a PCA based morphing algorithm. All anatomical measures and the envelope boundaries at 10°, 50° and 100° (green asterisk) were used for the envelope and gait prediction. Mean RMS error for the envelope prediction was 0.5° and for the gait prediction was 1.7°.

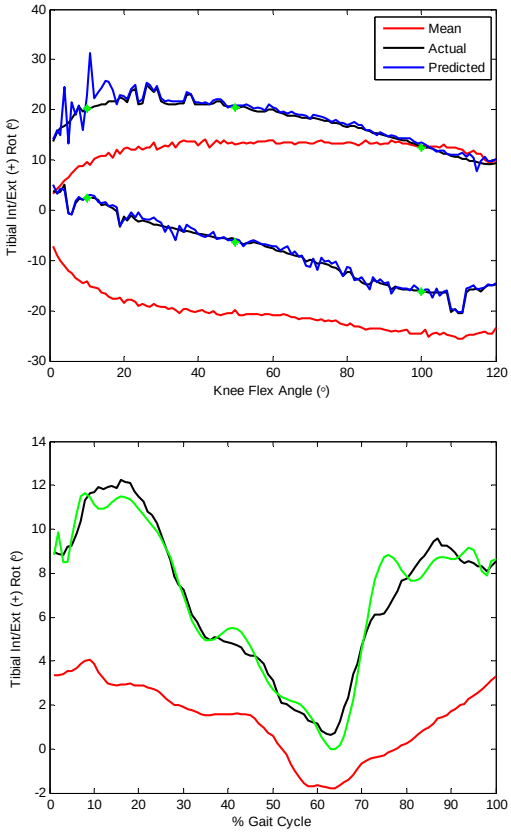

Figure 5.6: Mean (red), experimentally collected (black) and predicted (green) I-E motion of a random knee during envelope (top) and gait (bottom). Predictions were performed using a PCA based morphing algorithm. All anatomical measures and the envelope boundaries at 10°, 50° and 100° (green asterisk) were used for the envelope and gait prediction. Mean RMS error for the envelope prediction was 2.4° and for the gait prediction was 1.4°.

5.6 Tables

Table 5.1: Percentage variation in the anatomy, implant orientation, envelope and gait kinematics explained by first few PCs along with their interpretation. Two separate models were developed for V-V and I-E motions. Four PCs explained about 95% of the variation for the V-V dataset, whereas, three PCs explained 91.3% variation in the I-E dataset. FPA and TPA: Frontal and Transverse plane angle of epicondylar axis

	Principal components			**Variation Interpretation**			
	PC	**Variance**	**Cumulative**	**Envelope**	**Gait**	**Anatomical Factor**	**Implant Orientation**
V-V	PC1	50.9	50.9	shift	Shift of a motion	FPA, S-I location of lateral EpA and LCL origin	Femoral I-E rotation
	PC2	24.2	75.1	Size	Magnitude of range of motions	EpW, M-L location of both MCL and LCL	Tibial V-V rotation
	PC3	11.8	86.9	Envelope size in mid-flexion	Range during swing phase	A-P location of both MCL and LCL	Femoral F-E rotation
	PC4	8.6	95.5	Varus shift during early flexion	Varus shift during stance phase	S-I location of both med and lateral EpA	Tibial I-E rotation
I-E	PC1	50.6	50.6	shift	Shift of a motion	TPA, A-P location of lateral EpA, A-P location of LCL origin	Tibial I-E rotation
	PC2	34.7	85.3	Size	Magnitude of range of motion and temporal shift of peak internal rotation	EpW, M-L location of both MCL and LCL	Femoral I-E rotation
	PC3	6.0	91.3	Envelope size in mid-flexion	Range during swing phase	S-I location of both MCL and LCL	Femoral F-E rotation
	PC4	3.7	95.0	Internal shift in early flexion	Internal shift during stance phase	A-P location of MCL	Tibial V-V slope

Table 5.2: Mean RMS error (°) for the envelope and gait predictions of V-V and I-E motions. For each knee, envelope and gait kinematics was predicted and later compared with the actual kinematics.

Knee	VV		IE	
	Envelope	Gait	Envelope	Gait
1	0.93	0.34	0.17	0.88
2	0.39	0.20	0.32	0.98
3	0.79	0.61	1.07	1.21
4	0.63	0.55	0.41	0.75
5	2.58	2.56	1.02	1.01
6	0.35	0.26	1.10	1.11
7	0.66	0.67	0.30	0.80
8	0.56	0.22	0.15	1.02
9	0.50	1.72	2.38	1.47
10	1.23	1.21	1.57	1.58

Appendix A

The algorithm was developed and explained by the Styner *et al*. For PCA the mean model is the most probable surface. Therefore, the 'most probable surface' which satisfies the boundary conditions would be the surface which has minimal deviation from the mean. This objective function can be satisfied by minimizing the Mahalanobis-distance D_m.

To determine the most probable surface given the position of an arbitrary point *j*, the minimally Mahalanobis-distant surface $\vec{b}$ that contains the point *j* at the required position p_j must be found. So for all possible displacements p_j, a shape vector ϵ span(U) which translates the point *j* in direction (in the object space) would be seek, thereby only inducing a minimal deformation of the overall surface. More precisely, the shape vector shall be effect a unit displacement of the vertex *j* in the direction of a data point, and, as there are probably many such vectors, they shall be of minimal Mahalanobis-length D_m. Once the vector is found, one can satisfy all possible boundary conditions p_j with minimal deformation of the surface by just adding the appropriately weighted “basis" vector to the mean. This problem gives rise to the following constrained optimization:

Let $\boldsymbol{r}_j$ denote the unknown basis vector causing unit translation of point *j*. The mahalanobis-length D_m of this vector then given by:

$$D_m(\boldsymbol{r_k}) = (U_{r_k})^T \sum^{-1} U_{r_k} = r_k^T \wedge^{-1} r_k = \sum_{e=1}^{N-1} \frac{(r_k^{[e]})^2}{\lambda_e},\ k \epsilon \{x_j\}$$

Where, $\sum$ = covariance matrix

U = Eigenvectors

$\wedge$ = Diagonal matrix of eigenvalues

λ = Eigenvalue

Taking into account that x_j depend only on a row of U, Sub-matrix U_j is obtained from the following equation:

$$\left[xj\right]=\left[\overline{xj}\right]+\left[U^{j}\right]b=\left[\overline{xj}\right]+U^{j}b$$

Where, $U^j = J^{th}$ row of matrix U.

$b = U^T * P$ ... P = *Data matrix.*

To minimize the mahalonobis-distance D_m subject to the constraint of a decoupled translation by one unit, Lagrange function was introduced. This constrained optimization routine was solved using a Lagrange function (L_j) by Styner *et al*.

If the basis vectors and the Lagrange multiplier is combined according to $R_j = [r_j]$,

$$2\wedge^{-1} R_j = U_j^T L_j \ldots\ldots\ldots\ldots (1)$$

$$U_j R_j = I \ldots\ldots\ldots\ldots (2)$$

If r_j is the basis vector, then result from simple algebraic operations (resolve (1) for R_j and replace R_j in (2) by the result), use the resulting equation to find $L_j = 2\left[U_j \wedge U_j^T\right]^{-1}$. Substitute for L_j in (1) and R_j is given by:

$$R_j = [r_{x_j}] = \wedge U_j^T\left[U_j \wedge U_j^T\right]^{-1}$$

While, r_j , describes the translation of x_j by one unit. The most probable surface $\tilde{p}$ given the displacement $[\Delta x]$ of an arbitrary data point j is then determined by,

$$\tilde{p} = \overline{p} + UR_j[x_j]$$

Before the next control point is considered, one must ensure that the subsequent modifications will not alter the previously obtained data and thus the components from the statistic that caused a displacement from previous point were removed. The variation coded by the point was subtracted from each instance *i*, and rebuild the statistic afterwards. For the first part of this operation, the basis vectors R_j weighted by the specific displacement $[\Delta x_j]^T_i$ was subtracted from each object instance

$$\tilde{b_i^j} = b_i - R_j\left[\Delta x_j\right] = b_i - R_j U_j b_i = (I - R_j U_j) b_i$$

Where, $b_i = U^T \Delta p_i$ and $\Delta p_i = p_i - \overline{p}$

After this step, a new data description that is invariant with respect to point *j* is obtained. In order to rebuild the statistic, a PCA to the normalized data $\{\tilde{b_i^j} \mid i \in \{1,...,N\}\}$ was applied. The point-normalized principal components, denoted by U^j, confirm the expected behavior and validate the removal of the variation in respect of point *j*.

The final most probable surface $\tilde{p}_l$ is given by reversing the point elimination procedure, that is, by combining the data information that is coded by the various control points. Accordingly, the mean surface $\overline{p}$ with all the weighted principal basis functions $R_{j_k}^{\tilde{s}_{k-1}}$ was combined

$$\tilde{p}_l = \overline{p} + \sum_{k=1}^{l} U^{\tilde{s}_{k-1}} R_{j_k}^{\tilde{s}_{k-1}} \left[\Delta x_{j_k}\right]$$

Therefore, final recursive data, $\tilde{p}_k$, will be obtained by,

$$\tilde{p}_k = \overline{p}_{k-1} + U^{\tilde{S}_{k-1}} R_{j_k}^{\tilde{s}_{k-1}} \left[\Delta x_{j_k}\right]$$

Chapter 6: Conclusion and Future Work

Kinematics variation is the inheritant part of the joint mechanics; factors such as patient anatomy, joint loading, implant alignment and neuromuscular feedbacks are all variable in nature. As stated in the Introduction, purpose of the current research was to combine experimental methodology with statistical models to understand the variation in passive knee envelope, anatomy, implant alignment and functional kinematics. These models could then be used to assist surgeons in making intra-operative decisions. Research summarized in the previous chapters ensures an important step towards the goal.

Chapter 3 described a methodology to perform passive knee envelope assessment and develop PCA model. This study demonstrated the capability of PCA and its application to identify modes of variation in the passive knee envelope. In recent years, navigation systems such as CAS have been gaining popularity [40]. Surgeons can perform and collect tibiofemoral kinematics during intra-surgery passive knee envelope. Combined with knee kinematics collected by a CAS system, the PCA methodology developed in Chapter 3 could be used to obtain patient-specific passive knee characteristics.

This modeling methodology offers an opportunity to further understand the variation in active motion paths and their relationship with various anatomical factors. The PCA model developed in Chapter 4 shed light on the relationship between passive knee envelope, knee anatomy and functional kinematics during gait. Furthermore, a PCA based morphing algorithm can predict the entire envelope and gait kinematics using anatomical factors and a subset of envelope measures. Results obtained in the current study, provides the relationship of anatomy and passive envelope with active kinematics. Although during surgery, surgeons do not have a priori knowledge about the patient's kinematics during functional activities, passive knee

assessment is usually performed. Surgeons could potentially use MRI to get the anatomical features and use passive knee envelope at certain flexion angles and predict entire patient-specific envelope and kinematics during functional activities.

Chapter 5 demonstrates the ability of a PCA model to explain relationship between knee anatomy, implant alignment, post-TKA envelope and kinematics during gait. During surgery, surgeons follow several philosophies to find optimum alignment of the implant. Numerous *in vivo* and *in vitro* studies have been performed to understand the influence of implant alignment on the kinematics [36, 38, 39, 86, 92]. In recent years, navigational systems have been using algorithms to predict femoral and tibial implant alignments before securing them on the bone. These implant alignments along with the anatomical and a few envelope features can be used to predict the post-TKA kinematics. In the current study, all implant alignments were described relative to the Grood and Suntay femoral and tibial coordinate frames. Previous research has demonstrated that the femoral coordinate frames developed using Grood and Suntay description are more precise [90]. However, inter and intra-prober error in indentifying the land marks could reflect in the implant alignment features.

Previous research has shown the effects of inter and intra-prober variation in identifying anatomical landmark on the kinematics [74, 90, 91]. Variation in the anatomical coordinate frame definition could essentially result into the different magnitude of I-E and V-V motion at the start point. Kinematics data used in Chapter 3 was normalized to the mid-point of the envelope at full extension. Whereas, kinematics dataset used in Chapter 4 and Chapter 5 was non-normalized absolute data. Despite this, major mode of variation (PC1) in both normalized and non-normalized dataset was the shift in the envelope and gait kinematics. The observation

indicates that the shift in envelope and gait kinematics, variation explained by the first PC, was not caused due to the variation in anatomical coordinate frame definition.

In the reported research, three separate set of PC models were developed; first, only passive envelope, second, anatomy-passive envelope-gait and third, anatomy-implant alignment-envelope-gait. These studies summarized how a few anatomical and implant alignment factors affected the kinematics; however, it was difficult to distinguish the effects of anatomical factors and implant orientation on the kinematics individually. Also, in these three models, maximum variation in the tibiofemoral kinematics, during envelope and gait, was due to its shift, whereas, second maximum variation was due to the envelop size and the gait ROM. Although other variables such as EpW, its orientation and implant alignment showed their influence on the kinematics, the role played by them individually was not calculated.

In a recently published study, Laz *et al*. developed a methodology to calculate contribution of patellar implant alignment variables on each PC [93]. Models developed in this study could be further developed to estimate contribution of each variable on the kinematics. Another option would be to perform envelope and gait prediction using all the variables and then by eliminating one variable at a time. There exists sufficient experimental data in the dataset used for Chapter 3, 4 and 5 to perform such a predictions, which could potentially help understand the role played by individual factor in the output kinematics. Also, achieved maximum and minimum envelope boundaries at 10º, 50º and 100º of knee flexion were used for gait predictions. Extensive design of experiment approach can be used to observe the effect of envelope boundaries at different flexion angles on the predictions.

Finally, envelope and gait predictions were more accurate for the post-surgery PCA models than the natural PCA models. For both natural and post-surgery models, the collateral origins and

the epicondylar width, a knee size measure, were the only anatomical factors considered. Origin locations of the cruciates were difficult to measure and were not included in the study. Numerous studies have reported variation in the natural tibial posterior slope [16, 43, 94]. Blankevoort *et al.* measured slope of the medial and lateral tibial plateau [16]. The group concluded that the tibial posterior slope was not only significantly different between the medial and lateral plateau, but also across the gender and ethnicity. Previous research has demonstrated a positive relationship between the epicondylar width and other tibiofemoral size variables; however, relationship of epicondylar width with tibial slope is not reported in the literature. In this study, natural PCA models did not include the cruciate origins and the tibial posterior slope, which may have affected their prediction accuracy. In post-surgery PCA models, the tibial posterior slope, along with a few other implant orientation factors, was included. Furthermore, during surgery, both cruciate ligaments were sacrificed (∑ PS Fixed, DePuy Inc.). So, compared to natural PCA models, post-TKA models used more 'complete' information.

An understanding of the impact of the anatomy and implant alignment variable on the kinematics can provide guidance to concentrate on those variables of the primary concern. Overall, this work demonstrated the ability of PCA as a methodology to interpret multivariate kinematics. Furthermore, the models developed here shed light on the relationship between a subset of knee anatomical features, implant alignment, envelope and functional kinematics during gait. The combine experimental and PCA approach can serve as a tool, which can account for various sources of variation in the dataset and assist the knee implant designers and surgeons.

References

1. Beynnon, B., J. Yu, D. Huston, B. Fleming, R. Johnson, L. Haugh, and M.H. Pope, *A sagittal plane model of the knee and cruciate ligaments with application of a sensitivity analysis.* J Biomech Eng, 1996. **118**(2): p. 227-39.
2. Blankevoort, L., R. Huiskes, and A. de Lange, *Recruitment of knee joint ligaments.* J Biomech Eng, 1991. **113**(1): p. 94-103.
3. Blankevoort, L., R. Huiskes, and A. de Lange, *The envelope of passive knee joint motion.* J Biomech, 1988. **21**(9): p. 705-20.
4. Bertozzi, L., R. Stagni, S. Fantozzi, and A. Cappello, *Knee model sensitivity to cruciate ligaments parameters: a stability simulation study for a living subject.* J Biomech, 2007. **40 Suppl 1**: p. S38-44.
5. Nakamura, N., M. Ellis, and B.B. Seedhom, *Advancement of the tibial tuberosity. A biomechanical study.* J Bone Joint Surg Br, 1985. **67**(2): p. 255-60.
6. Walker, P.S., C.J. Wang, and Y. Masse, *Joint laxity as a criterion for the design of condylar knee prostheses. 1974.* Clin Orthop Relat Res, 2003(410): p. 5-12.
7. Mensch, J.S. and H.C. Amstutz, *Knee morphology as a guide to knee replacement.* Clin Orthop Relat Res, 1975(112): p. 231-41.
8. Rooney, N., D.P. Fitzpatrick, and D.E. Beverland, *Intraoperative knee anthropometrics: correlation with cartilage wear.* Proc Inst Mech Eng [H], 2006. **220**(6): p. 671-5.
9. Iwaki, H., V. Pinskerova, and M.A. Freeman, *Tibiofemoral movement 1: the shapes and relative movements of the femur and tibia in the unloaded cadaver knee.* J Bone Joint Surg Br, 2000. **82**(8): p. 1189-95.
10. Martelli, S. and V. Pinskerova, *The shapes of the tibial and femoral articular surfaces in relation to tibiofemoral movement.* J Bone Joint Surg Br, 2002. **84**(4): p. 607-13.
11. Fitzpatrick, C.K., D.P. FitzPatrick, and D.D. Auger, *Size and shape of the resection surface geometry of the osteoarthritic knee in relation to total knee replacement design.* Proc Inst Mech Eng [H], 2008. **222**(6): p. 923-32.
12. Mahfouz, M.R., *Analysis of Variation and Automated Measurement of Adult Femur Using Sex-Specific Atlas*, in *Americal Academy of Orthopaedic Surgeons*2007.
13. Fleute, M., S. Lavallee, and R. Julliard, *Incorporating a statistically based shape model into a system for computer-assisted anterior cruciate ligament surgery.* Med Image Anal, 1999. **3**(3): p. 209-22.
14. Hill, P.F., V. Vedi, A. Williams, H. Iwaki, V. Pinskerova, and M.A. Freeman, *Tibiofemoral movement 2: the loaded and unloaded living knee studied by MRI.* J Bone Joint Surg Br, 2000. **82**(8): p. 1196-8.
15. Nakagawa, S., Y. Kadoya, S. Todo, A. Kobayashi, H. Sakamoto, M.A. Freeman, and Y. Yamano, *Tibiofemoral movement 3: full flexion in the living knee studied by MRI.* J Bone Joint Surg Br, 2000. **82**(8): p. 1199-200.
16. de Boer, J.J., L. Blankevoort, I. Kingma, and W. Vorster, *In vitro study of inter-individual variation in posterior slope in the knee joint.* Clin Biomech (Bristol, Avon), 2009. **24**(6): p. 488-92.
17. Aoife and D. Fitzpatrick, *Anatomical Variation Associated with a Knee Joint.* 2008.
18. Yao, J., S.L. Lancianese, K.R. Hovinga, J. Lee, and A.L. Lerner, *Magnetic resonance image analysis of meniscal translation and tibio-menisco-femoral contact in deep knee flexion.* J Orthop Res, 2008. **26**(5): p. 673-84.

19. Amiri, S., D. Cooke, I.Y. Kim, and U. Wyss, *Mechanics of the passive knee joint. Part 1: The role of the tibial articular surfaces in guiding the passive motion.* Proc Inst Mech Eng [H], 2006. **220**(8): p. 813-22.
20. Engh, G.A., *The difficult knee: severe varus and valgus.* Clin Orthop Relat Res, 2003(416): p. 58-63.
21. John, G., *The Mechanics of the Knee and Prosthesis Design.* ORS, Las Vegas, 1977.
22. Wilson, D.R., J.D. Feikes, and J.J. O'Connor, *Ligaments and articular contact guide passive knee flexion.* J Biomech, 1998. **31**(12): p. 1127-36.
23. Wasielewski, R.C., D.D. Galat, and R.D. Komistek, *Correlation of compartment pressure data from an intraoperative sensing device with postoperative fluoroscopic kinematic results in TKA patients.* J Biomech, 2005. **38**(2): p. 333-9.
24. Zihlmann, M.S., A. Stacoff, J. Romero, I.K. Quervain, and E. Stussi, *Biomechanical background and clinical observations of rotational malalignment in TKA: literature review and consequences.* Clin Biomech (Bristol, Avon), 2005. **20**(7): p. 661-8.
25. Matsumoto, T., H. Muratsu, N. Tsumura, K. Mizuno, R. Kuroda, S. Yoshiya, and M. Kurosaka, *Joint gap kinematics in posterior-stabilized total knee arthroplasty measured by a new tensor with the navigation system.* J Biomech Eng, 2006. **128**(6): p. 867-71.
26. Matsueda, M., T.R. Gengerke, M. Murphy, W.D. Lew, and R.B. Gustilo, *Soft tissue release in total knee arthroplasty. Cadaver study using knees without deformities.* Clin Orthop Relat Res, 1999(366): p. 264-73.
27. Unitt, L., A. Sambatakakis, D. Johnstone, and T.W. Briggs, *Short-term outcome in total knee replacement after soft-tissue release and balancing.* J Bone Joint Surg Br, 2008. **90**(2): p. 159-65.
28. Kupper, J.C., B. Loitz-Ramage, D.T. Corr, D.A. Hart, and J.L. Ronsky, *Measuring knee joint laxity: a review of applicable models and the need for new approaches to minimize variability.* Clin Biomech (Bristol, Avon), 2007. **22**(1): p. 1-13.
29. Ozkan, M., N.E. Akalan, and Y. Temelli, *Interaction of ligament bundles and articular contacts for the simulation of passive knee flexion.* Conf Proc IEEE Eng Med Biol Soc, 2007. **2007**: p. 4297-300.
30. Papannagari, R., L.E. DeFrate, K.W. Nha, J.M. Moses, M. Moussa, T.J. Gill, and G. Li, *Function of posterior cruciate ligament bundles during in vivo knee flexion.* Am J Sports Med, 2007. **35**(9): p. 1507-12.
31. Akalan, N.E., M. Ozkan, and Y. Temelli, *Three-dimensional knee model: constrained by isometric ligament bundles and experimentally obtained tibio-femoral contacts.* J Biomech, 2008. **41**(4): p. 890-6.
32. Park, S.E., L.E. DeFrate, J.F. Suggs, T.J. Gill, H.E. Rubash, and G. Li, *Erratum to "The change in length of the medial and lateral collateral ligaments during in vivo knee flexion".* Knee, 2006. **13**(1): p. 77-82.
33. !!! INVALID CITATION !!!
34. Binazzi, R., M. Soudry, L.A. Mestriner, and J.N. Insall, *Knee arthroplasty rating.* J Arthroplasty, 1992. **7**(2): p. 145-8.
35. D'Lima, D.D., N. Steklov, B.J. Fregly, S.A. Banks, and C.W. Colwell, Jr., *In vivo contact stresses during activities of daily living after knee arthroplasty.* J Orthop Res, 2008. **26**(12): p. 1549-55.
36. Siston, R.A., S.B. Goodman, S.L. Delp, and N.J. Giori, *Coronal plane stability before and after total knee arthroplasty.* Clin Orthop Relat Res, 2007. **463**: p. 43-9.

37. Tanaka, K., H. Muratsu, K. Mizuno, R. Kuroda, S. Yoshiya, and M. Kurosaka, *Soft tissue balance measurement in anterior cruciate ligament-resected knee joint: cadaveric study as a model for cruciate-retaining total knee arthroplasty.* J Orthop Sci, 2007. **12**(2): p. 149-53.
38. Berger, R.A., H.E. Rubash, M.J. Seel, W.H. Thompson, and L.S. Crossett, *Determining the rotational alignment of the femoral component in total knee arthroplasty using the epicondylar axis.* Clin Orthop Relat Res, 1993(286): p. 40-7.
39. Anouchi, Y.S., L.A. Whiteside, A.D. Kaiser, and M.T. Milliano, *The effects of axial rotational alignment of the femoral component on knee stability and patellar tracking in total knee arthroplasty demonstrated on autopsy specimens.* Clin Orthop Relat Res, 1993(287): p. 170-7.
40. Picard, F., A.H. Deakin, J.V. Clarke, J.M. Dillon, and A. Gregori, *Using navigation intraoperative measurements narrows range of outcomes in TKA.* Clin Orthop Relat Res, 2007. **463**: p. 50-7.
41. Dennis, D.A., R.D. Komistek, G.R. Scuderi, and S. Zingde, *Factors affecting flexion after total knee arthroplasty.* Clin Orthop Relat Res, 2007. **464**: p. 53-60.
42. Sharma, A., R.D. Komistek, C.S. Ranawat, D.A. Dennis, and M.R. Mahfouz, *In vivo contact pressures in total knee arthroplasty.* J Arthroplasty, 2007. **22**(3): p. 404-16.
43. Shelburne, K.B., M.R. Torry, and M.G. Pandy, *Contributions of muscles, ligaments, and the ground-reaction force to tibiofemoral joint loading during normal gait.* J Orthop Res, 2006. **24**(10): p. 1983-90.
44. Lubowitz, J.H., B.J. Bernardini, and J.B. Reid, 3rd, *Current concepts review: comprehensive physical examination for instability of the knee.* Am J Sports Med, 2008. **36**(3): p. 577-94.
45. Markolf, K.L., W.L. Bargar, S.C. Shoemaker, and H.C. Amstutz, *The role of joint load in knee stability.* J Bone Joint Surg Am, 1981. **63**(4): p. 570-85.
46. ISO-14243-1, *Loading and displacement parameters for wear-testing machines with load control and corrosponding environment conditions for test.* 2002.
47. Schipplein, O.D. and T.P. Andriacchi, *Interaction between active and passive knee stabilizers during level walking.* J Orthop Res, 1991. **9**(1): p. 113-9.
48. Joliffe, I.T., *Principal Component Analysis.* Springers Series of Statistics, 2002.
49. Deluzio, K.J. and J.L. Astephen, *Biomechanical features of gait waveform data associated with knee osteoarthritis: an application of principal component analysis.* Gait Posture, 2007. **25**(1): p. 86-93.
50. Deluzio, K.J., U.P. Wyss, and B. Zee, *Gait Assessment in Unicompartmental Knee Arthroplasty Patients: PC Modeling of a Gait Waveform and Clinical Status.* Human Movement Science, 1999. **1999**(18): p. 791-711.
51. Epifanio, I., C. Avila, A. Page, and C. Atienza, *Analysis of multiple waveforms by means of functional principal component analysis: normal versus pathological patterns in sit-to-stand movement.* Med Biol Eng Comput, 2008. **46**(6): p. 551-61.
52. Sadeghi, H., F. Prince, S. Sadeghi, and H. Labelle, *Principal component analysis of the power developed in the flexion/extension muscles of the hip in able-bodied gait.* Med Eng Phys, 2000. **22**(10): p. 703-10.
53. Sadeghi, H., P. Allard, F. Barbier, S. Sadeghi, S. Hinse, R. Perrault, and H. Labelle, *Main functional roles of knee flexors/extensors in able-bodied gait using principal component analysis (I).* Knee, 2002. **9**(1): p. 47-53.

54. Jones, L., C.A. Holt, and M.J. Beynon, *Reduction, classification and ranking of motion analysis data: an application to osteoarthritic and normal knee function data.* Comput Methods Biomech Biomed Engin, 2008. **11**(1): p. 31-40.
55. Cootes, T.F., D.H. Cooper, and J. Grahsm, *Active Shape Models-Their Training and Application.* Computer Vision and Image Understanding, 1995. **61**(1): p. 38-59.
56. Aglietti, P., J.N. Insall, and G. Cerulli, *Patellar pain and incongruence. I: Measurements of incongruence.* Clin Orthop Relat Res, 1983(176): p. 217-24.
57. Wilson, D.R., J.D. Feikes, A.B. Zavatsky, and J.J. O'Connor, *The components of passive knee movement are coupled to flexion angle.* J Biomech, 2000. **33**(4): p. 465-73.
58. Maletsky, L.P., J. Sun, and N.A. Morton, *Accuracy of an optical active-marker system to track the relative motion of rigid bodies.* J Biomech, 2007. **40**(3): p. 682-5.
59. Grood, E.S. and W.J. Suntay, *A joint coordinate system for the clinical description of three-dimensional motions: application to the knee.* J Biomech Eng, 1983. **105**(2): p. 136-44.
60. Landry, S.C., K.A. McKean, C.L. Hubley-Kozey, W.D. Stanish, and K.J. Deluzio, *Knee biomechanics of moderate OA patients measured during gait at a self-selected and fast walking speed.* J Biomech, 2007. **40**(8): p. 1754-61.
61. Wrigley, A.T., W.J. Albert, K.J. Deluzio, and J.M. Stevenson, *Principal component analysis of lifting waveforms.* Clin Biomech (Bristol, Avon), 2006. **21**(6): p. 567-78.
62. Bradley, J., D. FitzPatrick, D. Daniel, T. Shercliff, and J. O'Connor, *Orientation of the cruciate ligament in the sagittal plane. A method of predicting its length-change with flexion.* J Bone Joint Surg Br, 1988. **70**(1): p. 94-9.
63. Johal, P., A. Williams, P. Wragg, D. Hunt, and W. Gedroyc, *Tibio-femoral movement in the living knee. A study of weight bearing and non-weight bearing knee kinematics using 'interventional' MRI.* J Biomech, 2005. **38**(2): p. 269-76.
64. Aglietti, P., J.N. Insall, R. Buzzi, and G. Deschamps, *Idiopathic osteonecrosis of the knee. Aetiology, prognosis and treatment.* J Bone Joint Surg Br, 1983. **65**(5): p. 588-97.
65. Griffin, F.M., J.N. Insall, and G.R. Scuderi, *The posterior condylar angle in osteoarthritic knees.* J Arthroplasty, 1998. **13**(7): p. 812-5.
66. Deluzio, K.J., U.P. Wyss, and B. Zee, *PC models of Knee Kinematics and Kinetics: Normal Vs. Pathological Gait Patterns.* Human Movement Science, 1997. **16**: p. 201-217.
67. Chester, V.L. and A.T. Wrigley, *The identification of age-related differences in kinetic gait parameters using principal component analysis.* Clin Biomech (Bristol, Avon), 2008. **23**(2): p. 212-20.
68. Rajamani K T, S.M., *Bone morphing with statistical shape models for enhanced visualization.* Proc of SPIE, 2004. **5367**: p. 122.
69. Maletsky, L.P. and B.M. Hillberry, *Simulating dynamic activities using a five-axis knee simulator.* J Biomech Eng, 2005. **127**(1): p. 123-33.
70. Bryan R, T.M., *Statistical modellinig of the whole human femur incorporating geomatrical and material properies.* Med Engg Phy, 2010. **32**: p. 57-65.
71. Booth, R.E., Jr., M.A. Freeman, D.S. Hungerford, J.N. Insall, S.D. Stulberg, and L.A. Whiteside, *Knee challenges: what would you do?* Orthopedics, 1997. **20**(9): p. 875-80.
72. Clarke, H.D., R. Fuchs, G.R. Scuderi, E.L. Mills, W.N. Scott, and J.N. Insall, *The influence of femoral component design in the elimination of patellar clunk in posterior-stabilized total knee arthroplasty.* J Arthroplasty, 2006. **21**(2): p. 167-71.

73. Easley, M.E., J.N. Insall, G.R. Scuderi, and D.D. Bullek, *Primary constrained condylar knee arthroplasty for the arthritic valgus knee.* Clin Orthop Relat Res, 2000(380): p. 58-64.
74. Morton N, M.L., Pal S, Laz P, *Effect of variability in anatomical landmark location on knee kinematic description.* J Orthop Res, 2007: p. 1227.
75. Insall, J.N., R. Binazzi, M. Soudry, and L.A. Mestriner, *Total knee arthroplasty.* Clin Orthop Relat Res, 1985(192): p. 13-22.
76. Insall, J.N. and M. Kelly, *The total condylar prosthesis.* Clin Orthop Relat Res, 1986(205): p. 43-8.
77. Ranawat, C.S., *The patellofemoral joint in total condylar knee arthroplasty. Pros and cons based on five- to ten-year follow-up observations.* Clin Orthop Relat Res, 1986(205): p. 93-9.
78. Innocenti, B., S. Pianigiani, L. Labey, J. Victor, and J. Bellemans, *Contact forces in several TKA designs during squatting: A numerical sensitivity analysis.* J Biomech, 2011. **44**(8): p. 1573-81.
79. Harris, J.D., K.K. Solak, R.A. Siston, A. Litsky, J. Richards, and D.C. Flanigan, *Contact pressure comparison of proud osteochondral autograft plugs versus proud synthetic plugs.* Orthopedics, 2011. **34**(2): p. 97.
80. Akagi, M., S. Mori, S. Nishimura, A. Nishimura, T. Asano, and C. Hamanishi, *Variability of extraarticular tibial rotation references for total knee arthroplasty.* Clin Orthop Relat Res, 2005(436): p. 172-6.
81. Fleute, M., *Building a Complete Surface Model from Sparce Data Using Statistical Shape Models: Application to CAS.* MICCAI, 1998.
82. Rajamani, K.T., Styner M, *Bone morphing with statistical shape models for enhanced visualization.* Medical Imaging: Visualization Image guided Procedures, 2004. **5367**: p. 122.
83. Standards, I., International Standard Organization, 14243-1:2002.
84. Miller, M.C., R.A. Berger, A.J. Petrella, A. Karmas, and H.E. Rubash, *Optimizing femoral component rotation in total knee arthroplasty.* Clin Orthop Relat Res, 2001(392): p. 38-45.
85. Hopgood, P., C.P. Martin, and P.J. Rae, *The effect of tibial implant size on post-operative alignment following medial unicompartmental knee replacement.* Knee, 2004. **11**(5): p. 385-8.
86. Thompson, J.A., M.W. Hast, J.F. Granger, S.J. Piazza, and R.A. Siston, *Biomechanical effects of total knee arthroplasty component malrotation: a computational simulation.* J Orthop Res, 2011. **29**(7): p. 969-75.
87. Martin, S.D., S.B. Haas, and J.N. Insall, *Primary total knee arthroplasty after patellectomy.* J Bone Joint Surg Am, 1995. **77**(9): p. 1323-30.
88. Insall, J.N., *Knee arthroplasty: then, now, and tomorrow.* Orthopedics, 1995. **18**(9): p. 889-92.
89. Griffin, F.M., K. Math, G.R. Scuderi, J.N. Insall, and P.L. Poilvache, *Anatomy of the epicondyles of the distal femur: MRI analysis of normal knees.* J Arthroplasty, 2000. **15**(3): p. 354-9.
90. Lenz, N.M., A. Mane, L.P. Maletsky, and N.A. Morton, *The effects of femoral fixed body coordinate system definition on knee kinematic description.* J Biomech Eng, 2008. **130**(2): p. 021014.

91. Langenderfer, J.E., P.J. Rullkoetter, A.G. Mell, and P.J. Laz, *A multi-subject evaluation of uncertainty in anatomical landmark location on shoulder kinematic description.* Comput Methods Biomech Biomed Engin, 2009. **12**(2): p. 211-6.
92. Scuderi, G.R., R.D. Komistek, D.A. Dennis, and J.N. Insall, *The impact of femoral component rotational alignment on condylar lift-off.* Clin Orthop Relat Res, 2003(410): p. 148-54.
93. Fitzpatrick, C.K., M.A. Baldwin, P.J. Rullkoetter, and P.J. Laz, *Combined probabilistic and principal component analysis approach for multivariate sensitivity evaluation and application to implanted patellofemoral mechanics.* J Biomech, 2011. **44**(1): p. 13-21.
94. Hashemi, J., N. Chandrashekar, B. Gill, B.D. Beynnon, J.R. Slauterbeck, R.C. Schutt, Jr., H. Mansouri, and E. Dabezies, *The geometry of the tibial plateau and its influence on the biomechanics of the tibiofemoral joint.* J Bone Joint Surg Am, 2008. **90**(12): p. 2724-34.